J. Fluid Mech. (2004), *vol.* 501, *pp.* 179–212.
DOI: 10.1017/S0022112003007468 Printed in the United Kingdom

The effects of hydraulic resistance on dam-break and other shallow inertial flows

By ANDREW J. HOGG[1] AND DAVID PRITCHARD[2]

[1]Centre for Environmental and Geophysical Flows, School of Mathematics, University of Bristol, Bristol BS8 1TW, UK
a.j.hogg@bris.ac.uk

[2]BP Institute for Multiphase Flow, University of Cambridge, Madingley Rise, Cambridge CB3 0EZ, UK
david@bpi.cam.ac.uk

(Received 18 April 2003 and in revised form 22 August 2003)

The effects of resistive forces on unsteady shallow flows over rigid horizontal boundaries are investigated theoretically. The dynamics of this type of motion are driven by the streamwise gradient of the hydrostatic pressure, which balances the inertia of the fluid and the basal resistance. Drag forces are often negligible provided the fluid is sufficiently deep. However, close to the front of some flows where the depth of the moving layer becomes small, it is possible for drag to substantially influence the motion. Here we consider three aspects of unsteady shallow flows. First we consider a regime in which the drag, inertia and buoyancy (pressure gradient) are formally of the same magnitude throughout the entire current and we construct a new class of similarity solutions for the motion. This reveals the range of solution types possible, which includes those with continuous profiles, those with discontinuous profiles and weak shocks and those which are continuous but have critical points of transition at which the gradients may be discontinuous. Next we analyse one-dimensional dam-break flow and calculate how drag slows the motion. There is always a region close to the front in which drag forces are not negligible. We employ matched asymptotic expansions to combine the flow at the front with the flow in the bulk of the domain and derive theoretical predictions that are compared to laboratory measurements of dam-break flows. Finally we investigate a modified form of dam-break flow in which the vertical profile of the horizontal velocity field is no longer assumed to be uniform. It is found that in the absence of drag it is no longer possible to find a kinematically consistent front of the fluid motion. However the inclusion of drag forces within the region close to the front resolves this difficulty. We calculate velocity and depth profiles within the drag-affected region, and obtain the leading-order expression for the rate at which the fluid propagates when the magnitude of the drag force is modelled using Chézy, Newtonian and power-law fluid closures; this compares well with experimental data and provide new insights into dam-break flows.

1. Introduction

Naturally occurring flows such as rivers, tidal currents, turbidity and debris flows are often of a sufficiently low aspect ratio, here defined as the ratio of their depth to streamwise extent, that the fluid pressure adopts hydrostatic balance and their dynamics are controlled by forces which are parallel to the underlying boundary (see, for example, Parker 1976; Simpson 1997; Iverson 1997). Furthermore, in many

situations the effects of basal drag on these flows can be neglected and the motion is governed by a balance between fluid inertia and the streamwise pressure gradient. However, when the depth of the flowing layer becomes sufficiently small it is no longer possible to neglect drag and a complete description of the flow must include hydraulic resistance. In this contribution we study a series of flows over rigid, horizontal boundaries and we demonstrate how to calculate the influence of the basal drag. These flows are gravity-driven by the input of dense fluid (see, for example, Simpson 1997), and dam-break flows which arise when fluid is released from rest following the sudden removal of a vertical barrier (Ritter 1892). We note that there is a close connection between the two: dam-break flows can be equivalently treated as gravity-driven motion from a constant source of dense fluid (Hogg & Woods 2001).

Gravity currents arise due to the intrusion of dense fluid into a less dense surrounding fluid. The motion over a horizontal, rigid boundary is driven by the buoyancy force associated with the density difference between the source and surrounding fluids. For inertially dominated gravity currents there have been a number of studies of their motion (see, for example, Simpson 1997; Hoult 1972; Huppert & Simpson 1980) and there is a wide-range of environmental applications including the propagation of sea breezes, the intrusion of saline fluid into freshwater lakes and, if the density difference is due to suspended particulate matter, the motion of volcanic ash clouds. These flows have usually been modelled mathematically using shallow-layer theories (Hoult 1972; Rottman & Simpson 1983; Gratton & Vigo 1994). Hogg & Woods (2001) showed that while the initial motion of these flows may be independent of basal drag, the later stages become strongly influenced by drag forces. Their study examined the transition between these two regimes and established new models for the motion in which the drag balances the buoyancy forces. In an analogous study of flow through a sparse, porous matrix, Hatcher, Hogg & Woods (2000) found a similar transition and were able to experimentally verify the transition and the new solution for the motion. In this paper, by considering a source which delivers fluid at a time-dependent rate, we identify a regime in which the drag, pressure gradient and inertial terms are all of the same order of magnitude throughout the entire flow and so there is no transition between regimes. Instead we construct solutions that are valid for the entire motion.

The one-dimensional dam-break flow that arises following the sudden removal of a vertical barrier, behind which fluid is initially at rest, has been studied for many years (Ritter 1892; Whitham 1974). Not only is it an important paradigm problem in the fluid mechanics of nonlinear shallow inertial flows, but it has been reproduced in laboratory experiments and may be of significance in large-scale environmental flows (Bellos & Sakkas 1987; Stansby, Chegini & Barnes 1998; Capart & Young 1998). When drag is neglected there is an analytical solution to the governing shallow-water model of the flow (Ritter 1892); denoting the initial height of fluid behind the dam and gravitational acceleration by h_0 and g, respectively, the velocity of the flow varies linearly with distance from the dam, attaining a speed of $2\sqrt{gh_0}$ at the front, and the depth of the flow decreases quadratically towards the front (see § 4). While the drag forces may be neglected in the main body of the flow, they are non-negligible in the 'tip' region close to the front and act to reduce the speed of the front. Keulegan (1950), Dressler (1954) and Lauber & Hager (1998), amongst others, report experimental observations of the shape of the intruding front of fluid, its velocity and the effects of drag forces. The key observations are the retardation of the leading front of fluid and the change in the curvature of the profile, to develop a blunt-nosed flow. This problem has been analysed theoretically by Dressler (1952)

and Whitham (1955); Dressler (1952) employed a regular perturbation scheme based on the successive approximation of the 'outer' flow, away from the front, whereas Whitham (1955) employed an integral model of the 'tip' region in which drag is non-negligible and balanced the forces acting on it. In this study we employ matched asymptotic expansions in which an 'inner' drag-affected region around the tip is matched to an 'outer' region in which drag is negligible. This provides the spatial structure of the height and velocity fields near the front, together with the reduction of speed due to basal drag. This latter result is similar, but not identical, to the two previous studies, which employed more limited asymptotic techniques. The results are of use since dam-break flows are readily generated in the laboratory (Stansby *et al.* 1998; Lauber 1997) and are used regularly as tests of numerical calculations (see, for example, Bellos & Sakkas 1987) and as an idealized flow in engineering applications (Peregrine & Williams 2001; Pritchard & Hogg 2002).

We note that a similar approach has been employed to study the unsteady flow down slopes of Newtonian (Hunt 1987) and non-Newtonian fluids (Huang & Garcia 1998). Likewise, these flows are calculated by matching between the bulk of the flow and the 'tip' region. For these flows, however, the outer motion in the bulk of the flow is governed by a simple dynamical balance between gravitational acceleration and basal drag, with negligible variation of the fluid inertia. This balance emerges as an algebraic relationship between the height and velocity fields (Weir 1983) and matching can be achieved in terms of a single dependent variable. In this study of dam-break flows over a horizontal bed, the bulk flow is also governed by a simple wave equation, but matching between the tip and outer regions is more complicated and is enforced by simultaneously matching the height and velocity fields.

In this contribution, we extend the analysis of dam-break flow in a number of ways. First we formulate a model of the flow based on depth-averaging that includes the possibility of shear in the horizontal velocity profile. Even for flows in the absence of drag this significantly modifies the dam-break solution and we find that it is not possible to construct a consistent solution for the motion; rather, we find that it is necessary to include resistive forces. Furthermore we investigate different representations of the basal drag, including forms that represent the resistance associated with fluids of Newtonian and power-law rheology. This broadens the application of this work to include fluids such as debris, muds and concentrated suspensions (Iverson 1997; Ancey 2002).

The paper is organized as follows: we first formulate the problem using the shallow-water equations and derive the jump conditions across discontinuities in the flow (§ 2). We then analyse gravity-current flow for the special case in which the drag, pressure gradient and inertial forces are of equal magnitude (§ 3). Here we construct new similarity solutions for the motion and thus extend the analysis of Gratton & Vigo (1994) to include drag forces. This analysis also reveals the significance of flows with discontinuities and points of critical transition where the field variables remain continuous but have discontinuous gradients. Indeed the structure of these somewhat idealized flows provides analytical insight for subsequent sections of this study. In § 4 we analyse dam-break flow in which the dynamical balance varies in space and we employ matched asymptotic expansions to calculate the flow. The flows we calculate in this section are continuous but also exhibit a transition point where the gradients are discontinuous. Finally in § 5 we investigate modified dam-break flow and demonstrate how shear in the velocity profile affects the results. We compare our theoretical predictions with experimental observations in § 4 and § 5. A summary and some concluding comments are given in § 6.

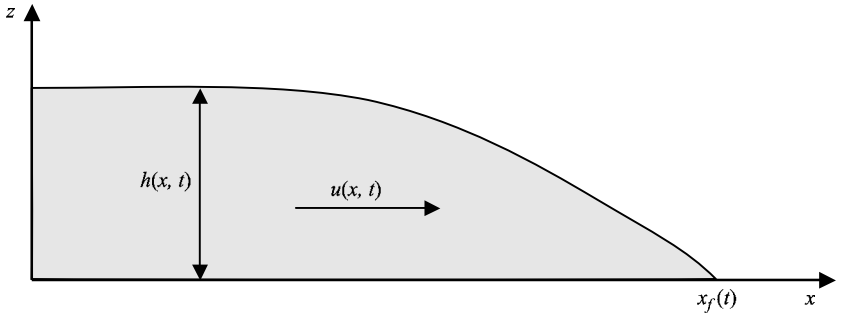

FIGURE 1. The configuration of the flow.

We also include an appendix in which drag is modelled as a Coulomb resistance. Such an approach has been applied to flows of debris (Iverson 1997) and granular materials (Savage & Hutter 1989). We demonstrate that the effects of drag are different in this case because they are uniform throughout the fluid domain.

2. Formulation

We consider a layer of fluid of density ρ, flowing over a rigid horizontal surface. The streamwise and vertical coordinates are denoted by x and z, respectively, and there is assumed to be no cross-stream variation so that the depth of the layer is given by $h(x,t)$ (see figure 1). On the assumption that the horizontal lengthscales of the motion, L, are much greater than the vertical lengthscales ($h/L \ll 1$), we find that vertical accelerations are negligible and the pressure adopts a hydrostatic distribution, given by

$$p = \rho g(h - z), \tag{2.1}$$

where p denotes the pressure field and g denotes gravitational acceleration. The assumption of a hydrostatic pressure leads to the shallow-water equations, which express conservation of mass and momentum (see, for example, Peregrine 1972; Whitham 1974). Denoting the horizontal velocity by u, mass conservation is given by

$$\frac{\partial h}{\partial t} + \frac{\partial}{\partial x}\int_0^h u \,\mathrm{d}z = 0. \tag{2.2}$$

Here we have assumed that the flowing shallow layer does not entrain fluid from its surroundings. Further, assuming that the top surface of the layer is stress-free and denoting the shear stress on the bottom surface by τ_b, the depth-integrated horizontal momentum equation may be written as

$$\frac{\partial}{\partial t}\int_0^h u \,\mathrm{d}z + \frac{\partial}{\partial x}\int_0^h u^2 \,\mathrm{d}z + \frac{\partial}{\partial x}\int_0^h \frac{p}{\rho}\,\mathrm{d}z = -\frac{\tau_b}{\rho}. \tag{2.3}$$

To complete this shallow-layer model we write

$$h\overline{u} = \int_0^h u \,\mathrm{d}z \quad \text{and} \quad \beta h\overline{u}^2 = \int_0^h u^2 \,\mathrm{d}z, \quad \text{where} \quad \beta = 1 + \frac{1}{h}\int_0^h \left(1 - \frac{u}{\overline{u}}\right)^2 \mathrm{d}z. \tag{2.4}$$

The coefficient β is often termed a shape factor. Its magnitude reflects the shear in the profile of the horizontal fluid velocity and may depend on factors such as the Reynolds number or the boundary roughness (Piau 1996). Although $\beta \geqslant 1$, it is frequently set equal to unity (Iverson 1997; Ancey 2002; Iverson & Denlinger 2001). We

demonstrate in § 5 that this may have a significant effect on the nature of the predicted flows.

Finally we relate the boundary shear stress, τ_b, to the height, velocity and mechanical properties of the fluid. Although the shear stress could be calculated in principle from the full governing equations, we adopt a common, much simpler approach and write semi-empirical expressions for the shear stress. This approach is used in depth-integrated models of rivers and estuaries (Parker 1976), turbidity currents (Parker, Fukushima & Pantin 1986) and mud flows (Coussot & Proust 1996; Mei, Liu & Yuhi 2002). If viscous effects are negligible we express the boundary shear stress in terms of the product of the fluid density ρ, the square of the horizontal velocity $\overline{u}$, and a Chézy drag coefficient C_D:

$$\tau_b = \rho C_D \overline{u}^2. \tag{2.5}$$

The magnitude of the drag coefficient is determined empirically but usually falls in the range 0.01–0.001 for most environmental flows (Parker 1976; Lewis 1997).

If, however, the drag arises through viscous interactions with the boundary, the shear stress is given by

$$\tau_b = c_1 \mu \overline{u}/h, \tag{2.6}$$

where μ is the dynamic viscosity and c_1 is a dimensionless constant. This model has been employed by Ng & Mei (1994) and is pursued in § 5. It can be generalized to express the drag associated with a fluid with power-law rheology. In this case

$$\tau_b = c_n \mu_n \left(\frac{\overline{u}}{h}\right)^n, \tag{2.7}$$

where μ_n is the viscosity coefficient and n is the flow index for the fluid, with $n = 1$ corresponding to a Newtonian fluid. In this expression c_n is a dimensionless constant. The analyses developed in § 4 and § 5 are independent of the precise values of the drag coefficient, C_D, the dimensionless constants c_n and the shape factor β. Indeed, we show in § 5 that it is not necessary to assume that β is constant throughout the flow. However, to illustrate the results, following Ng & Mei (1994) and Huang & Garcia (1998) we assume that the velocity field is given by

$$u(x, z, t) = \overline{u}(x, t)\frac{1+2n}{n+1}\left(1 - \left(1 - \frac{z}{h}\right)^{(n+1)/n}\right). \tag{2.8}$$

The profile satisfies no slip at the base and vanishing shear stress at the free surface. This assumption of vertical structure is similar to the approach employed by the von Kármán momentum integral in boundary layers (see, for example, Batchelor 1967). We anticipate that the results will not depend strongly on the precise vertical structure because a depth-integrated model is employed. However, we will show that the structure of the flows when the shape factor β is equal to unity is different from those for which β exceeds unity. Given the vertical structure (2.8), we find that

$$\beta = \frac{2(1+2n)}{2+3n} \qquad \text{and} \qquad c_n = \left(\frac{1+2n}{n}\right)^n. \tag{2.9}$$

Note that for shear-thinning fluids ($0 < n \leqslant 1$), the shape factor lies in the range $1 < \beta \leqslant 6/5$.

In the Appendix we consider an additional case, which occurs when we take $\beta = 1$ and a Coulomb drag term. This combination has been employed in studies of debris flows and granular avalanches, although the physical basis for such a model is less well developed than for simpler fluids.

The system of equations is hyperbolic and may admit discontinuous solutions. The flows either side of these weak shocks are connected by jump conditions which express conservation of mass and momentum across the moving discontinuity. Denoting the shock speed by c, these jump conditions are given by

$$[(\overline{u}-c)h]_{x=x_s^-}^{x=x_s^+}=0 \qquad \text{and} \qquad \left[\beta\overline{u}^2h-2\overline{u}ch+c^2h+\tfrac{1}{2}gh^2\right]_{x=x_s^-}^{x=x_s^+}=0, \tag{2.10}$$

where x_s is the position of the shock (Whitham 1974).

In this study, apart from a brief discussion in § 3, we do not impose any dynamic conditions at the front of the flow. Instead the front position emerges as part of the solution, where the height field vanishes. Thus, denoting the front position by $x_f(t)$, it satisfies

$$h(x_f,t)=0 \qquad \text{and} \qquad \frac{\mathrm{d}x_f}{\mathrm{d}t}=\overline{u}(x_f,t). \tag{2.11}$$

Initial conditions and source conditions depend upon the flow under consideration and will be introduced separately in each section. We note that this system of equations has been employed to model gravity current motion, which occurs when relatively dense fluid intrudes along a boundary under less dense fluid (Hogg & Woods 2001). For these flows, driven by the difference density, $\Delta\rho$, between the two fluids, gravity g is replaced by reduced gravity, $g'\equiv\Delta\rho g/\rho$.

In the analyses that follow, for notational clarity, the over-bar notation is dropped and the velocity field $u(x,t)$ henceforth denotes the depth-averaged velocity field.

3. Gravity currents with inertia, buoyancy and drag

Gravity currents flowing over horizontal boundaries have usually been modelled using the depth-integrated shallow-water equations (2.2) and (2.3) with $\beta=1$ (see, for example, Hoult 1972; Rottman & Simpson 1983). The flows are generated by a source of dense fluid for which the volume flux per unit width is given by

$$uh=Q_\alpha t^{\alpha-1} \qquad \text{at} \qquad x=0, \tag{3.1}$$

where α and Q_α are constants. The Froude number at the source is given by

$$u/\sqrt{gh}=F_0 \qquad \text{at} \qquad x=0. \tag{3.2}$$

In this section in which $\beta=1$, it is assumed that the source Froude number, F_0, is greater than unity so that it is possible to maintain both the flux and Froude number conditions. For subcritical flow with $F_0<1$, the source Froude number condition is dropped as the source may be influenced by downstream conditions. We note that for flows with $\beta>1$, Garrett & Gerdes (2003) showed that the hydraulic control at which downstream conditions cannot influence upstream behaviour occurs at a Froude number less than unity.

The governing equations have been integrated by a number of investigators using both analytical and numerical techniques (Hoult 1972; Rottman & Simpson 1983; Hallworth, Hogg & Huppert 1998). In particular, in the absence of drag ($C_D=0$) it is possible to construct similarity solutions for the motion, which provide useful intermediate asymptotics and have been borne out by experimental realizations of the flows (Huppert & Simpson 1980). Gratton & Vigo (1994) have systematically constructed the solutions for a range of conditions at the source ($0\leqslant\alpha<4$). They identify four different types of solution for the height and velocity fields. These are continuous, discontinuous, continuous with a critical transition and discontinuous

with a critical transition. When the drag is non-vanishing, the flow at sufficiently early times is only weakly affected by drag. Conversely, at later times the dynamics may be controlled by a balance between drag and the streamwise pressure gradient (Hogg & Woods 2001). In this section we study flows for which inertia, buoyancy and drag are all formally of the same magnitude. This analysis is analogous to the approach recently adopted by Acton, Huppert & Worster (2001), who in a different physical context examined a dynamical regime in which three physical effects were formally of the same order of magnitude. They found that the form of solutions possible in this somewhat idealized scenario yielded significant insight into the general nature of the flow. In this section we pursue the same approach before, in subsequent sections, analysing flows in which the dominant dynamical balance varies spatially.

To establish this regime, we first employ scaling analysis to determine α and then we construct a similarity solution. Balancing the inertia, pressure gradient and drag yields

$$\frac{u}{t} \sim \frac{gh}{x_f} \sim \frac{C_D u^2}{h}. \tag{3.3}$$

The volume flux at the source implies that

$$uh \sim Q_\alpha t^{\alpha-1}, \tag{3.4}$$

and for kinematic consistency we requite $u \sim x_f/t$. Thus we deduce that the three terms of (3.3) can only be of the same magnitude for all time if $\alpha = 4$. Hence we seek a similarity solution of the form

$$x_f = \lambda (gQ)^{1/3} t^2, \tag{3.5}$$

$$u = 2\lambda (gQ)^{1/3} t U(y), \tag{3.6}$$

$$h = 4\lambda^2 \left(\frac{Q^2}{g}\right)^{1/3} t^2 H(y), \tag{3.7}$$

where $y = x/x_f$ and λ, $H(y)$ and $U(y)$ are to be determined. A similarity solution of this form is valid provided that the aspect ratio of the flow remains sufficiently small that vertical accelerations are negligible and the pressure adopts a hydrostatic distribution. Thus we require that

$$\Omega \equiv \left(\frac{Q}{g^2}\right)^{1/3} \ll 1. \tag{3.8}$$

Sources with volume fluxes depending on t^4 were excluded by Gratton & Vigo (1994) on the assumption that small aspect ratios could not be satisfied for all time. Nevertheless, provided (3.8) is satisfied the solutions remain formally valid. On substituting (3.5)–(3.7) into the governing equations, we obtain

$$H - yH' + (UH)' = 0, \tag{3.9}$$

$$\tfrac{1}{2}U - yU' + UU' + H' = -\frac{C_D}{4\lambda\Omega}\frac{U^2}{H}, \tag{3.10}$$

where a prime denotes differentiation with respect to y. The sole dimensionless parameter is $\Lambda = C_D/\Omega$, which may be much greater, or much less, than unity, depending on the magnitude of the drag. The boundary conditions at the source are then given by

$$UH = 1/[2\lambda]^3 \qquad \text{and} \qquad U/H^{1/2} = F_0 \qquad \text{at} \quad y = 0, \tag{3.11}$$

provided the flow at the source is supercritical ($F_0 \geqslant 1$). At the front of the flow

$$H = 0 \qquad \text{and} \qquad U = 1 \qquad \text{at} \quad y = 1. \tag{3.12}$$

Flows with weak shocks may be constructed. The jump conditions for a shock at $y = y_s$ and shock speed $c = 2y_s t(gQ)^{1/3}$ are now given in terms of the similarity variables by

$$[(U - y_s)H]_{y=y_s^-}^{y=y_s^+} = 0 \qquad \text{and} \qquad \left[(U - y_s)^2 H + \tfrac{1}{2}H^2\right]_{y=y_s^-}^{y=y_s^+} = 0. \tag{3.13}$$

3.1. *Solutions in the absence of drag* ($C_D = 0$)

Guided by the study of Gratton & Vigo (1994) we expect solutions for $\alpha = 4$ to have the following forms: continuous; continuous with a critical transition, at which the gradients of $U(y)$ and $H(y)$ are discontinuous; and discontinuous. First we note a simple analytical solution for $F_0 = \sqrt{2}$, given by

$$U = 1 \qquad \text{and} \qquad H = \tfrac{1}{2}(1 - y). \tag{3.14}$$

For this case, we deduce that $\lambda = 2^{-2/3}$. By forming series expansions in the regime $|1 - y| \ll 1$, we expect all solutions to have the same form as (3.14). However, other source Froude numbers may be attained by introducing continuous or discontinuous transitions. We observe that the governing equations may be re-written as

$$[(U - y)^2 - H]H' = yH - \tfrac{1}{2}UH, \tag{3.15}$$

$$[(U - y)^2 - H]U' = H - \tfrac{1}{2}U(U - y). \tag{3.16}$$

Thus there may be solutions with discontinuous gradient if $(U - y)^2 - H = 0$ and $U = 2y$, simultaneously. For the solution given by (3.14), this occurs at $y = 1/2$ and we may construct continuous solutions with a discontinuous gradient at this transition point. These solutions are most readily constructed by forming series expansions around the transition point ($y = 1/2$). We find that two different expansions are possible, which lead to a range of solutions that correspond to a range of source Froude numbers between 1 and 2. For the solution with $F_0 = 2$, when $|y - 1/2| \ll 1$, the height and velocity fields are given by

$$H = \tfrac{1}{4} - \tfrac{1}{4}(y - 1/2) - \tfrac{3}{32}(y - 1/2)^2 + \ldots, \tag{3.17}$$

$$U = 1 - \tfrac{1}{2}(y - 1/2) - \tfrac{5}{16}(y - 1/2)^2 + \ldots. \tag{3.18}$$

Integrating to $y = 0$ yields $U(0) = 1.2$ and $H(0) = 0.36$. Alternatively we find an expansion in the regime $|y - 1/2| \ll 1$ of the form

$$U = 1 - 2a(1/2 - y)^{5/2} + \ldots, \tag{3.19}$$

$$H = \tfrac{1}{4} - \tfrac{1}{2}(y - 1/2) + a(1/2 - y)^{5/2} + \ldots, \tag{3.20}$$

where a is an arbitrary constant. Varying the magnitude of a corresponds to the solutions with $2 > F_0 \geqslant 1$.

Discontinuous solutions may be constructed for those flows with a source Froude number in excess of 2. For these source conditions we introduce a position y_s, with $y_s > 1/2$, at which the discontinuity occurs, and we use the jump conditions for mass and momentum to relate the solutions either side of the discontinuity. We plot the height and velocity fields for these similarity solutions in figure 2.

3.2. *Solutions with drag* ($C_D > 0$)

Flows with non-vanishing drag exhibit the same range of solutions as those presented above, depending on the magnitude of the source Froude number F_0 and the drag

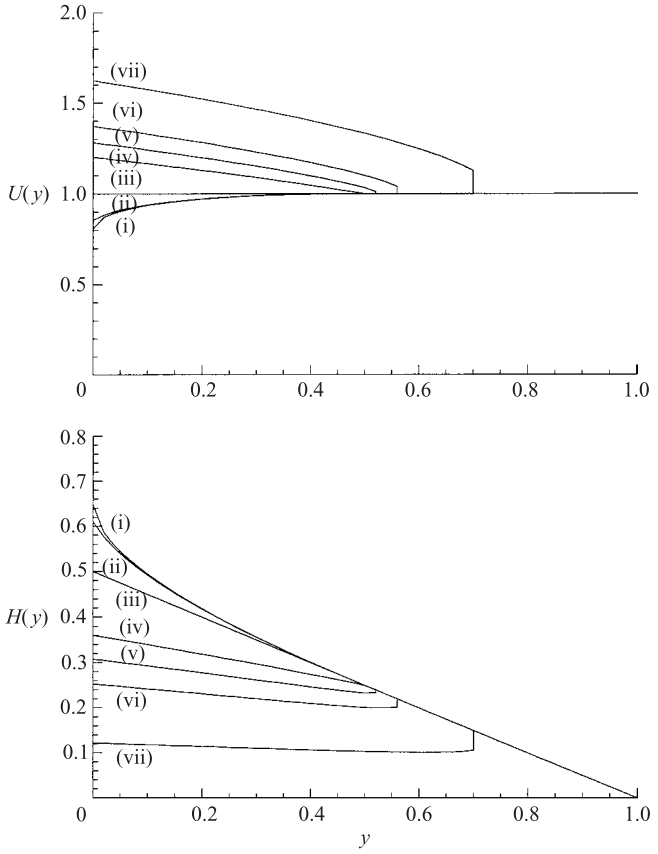

FIGURE 2. The similarity solutions for the height $H(y)$ and velocity $U(y)$ of an inertial gravity current in the absence of drag plotted as functions of the similarity variable y for various source Froude numbers: (i) $F_0 = 1$, $\lambda = 0.985$; (ii) $F_0 = 1.095$, $\lambda = 0.986$; (iii) $F_0 = 1.414$, $\lambda = 1$ (iv) $F_0 = 2$, $\lambda = 1.050$; (v) $F_0 = 2.309$, $\lambda = 1.106$; (vi) $F_0 = 2.789$, $\lambda = 1.130$; and (vii) $F_0 = 6.648$, $\lambda = 1.361$.

coefficient C_D (or Λ). In the region close to the front of the flow ($|1 - y| \ll 1$), the velocity and height take the form

$$H = \left[\frac{\Lambda}{2\lambda}(1-y)\right]^{1/2} + \ldots \qquad \text{and} \qquad U = 1 + \tfrac{1}{3}(1-y) + \ldots . \tag{3.21}$$

Thus the profiles of these drag-affected flows are rather different from those in the absence of drag: they are blunt nosed with $H(y) \sim (1-y)^{1/2}$, rather than adopting a linear profile close to the front. This arises because the motion at the front is most strongly affected by drag and so the current develops an increased streamwise pressure gradient to counter the resistance. This is analogous to the anatomy of a drag-affected current reported by Hogg & Woods (2001).

To analyse these flows we first note that if there exists a transition point ($y = y_c$) in the flow at which there are discontinuous gradients, then the height and velocity, denoted by H_c and U_c, respectively, are related by

$$H_c = (U_c - y_c)^2, \tag{3.22}$$

$$H_c(U_c - y_c) = \tfrac{1}{2}U_c H_c + \Lambda U_c^2/(4\lambda). \tag{3.23}$$

The transition point, y_c, occurs between 0 and $\frac{1}{2}$, with the limiting case $y_c = 0$ at $\Lambda = 1$ and $F_0 = 1$. Thus for $\Lambda > 1$ there are no points at which (3.22) and (3.23) are simultaneously satisfied, and apart from specific solutions with subcritical conditions at the source, only discontinuous solutions may be constructed.

When $0 < \Lambda < 1$, we seek series expansion for the height and velocity fields around the point $y = y_c$ in the form

$$H = H_c + a_1(y - y_c) + a_\gamma(y - y_c)^\gamma + \ldots, \tag{3.24}$$

$$U = U_c + b_1(y - y_c) + b_\gamma(y - y_c)^\gamma + \ldots, \tag{3.25}$$

where $a_1, b_1, a_\gamma, b_\gamma$ and γ are constants (and γ is assumed to be greater than unity). By substituting these series expansions into the governing equations and equating powers of $(y - y_c)$, we deduce that

$$a_1 = -(U_c - y_c)(b_1 + 1), \tag{3.26}$$

$$3b_1^2 + b_1\left(3 - 2\frac{y_c}{U_c} - \frac{y_c}{2(U_c - y_c)}\right) + \frac{U_c - 2y_c}{2(U_c - y_c)} = 0. \tag{3.27}$$

Furthermore we find that

$$a_\gamma = -(U_c - y_c)b_\gamma, \tag{3.28}$$

$$-3\gamma b_1 + \gamma - 3b_1 - 5/2 - \frac{(U_c - 2y_c)(3U_c - 2y_c)}{2U_c(U_c - y_c)} = 0, \tag{3.29}$$

and the constant a_γ is arbitrary. The quadratic equation (3.27) yields two solutions for b_1 and so from (3.29) we calculate two possible values of γ. However, one of the values is less than unity and so is inconsistent with the regime under consideration; for this value of γ we must set $a_\gamma = 0$. This series expansion leads to the continuous solution with the largest source Froude number given Λ; we denote this Froude number by $F_{0m}(\Lambda)$. For the other value of b_1 (and γ), a_γ remains an undetermined constant which may be chosen arbitrarily. Varying a_γ leads to continuous solutions with source Froude numbers in the range between unity and F_{0m}. Note that for $\Lambda = 0$, we find that the solution to (3.27) is given by $b_1 = 0$ or $b_1 = -1/2$, which leads to $\gamma = 5/2$ or $\gamma = 2/5$, respectively. We discount the root $\gamma = 2/5$ as this is inconsistent with our series expansion, which had assumed that $\gamma > 1$. Hence we have recovered the drag-free solutions presented in (3.18) and (3.19). We further find that when $\Lambda = 0$, $F_{0m} = 2$.

We plot the different solution regimes as a function of F_0 and Λ in figure 3 and note that continuous solutions are possible only for $1 \geqslant \Lambda \geqslant 0$ and $F_{0m}(\Lambda) \geqslant F_0 \geqslant 1$. (This regime includes solutions which are continuous and have continuous gradient — for example, when $\Lambda = 0$, this solution is given by (3.14).) For $\Lambda > 1$, only discontinuous supercritical solutions are possible, with the further restriction that $F_0 \geqslant F_{0s}(\Lambda)$. This lower bound on the source Froude number corresponds to having a shock at the source ($y = 0$). There are, however, continuous subcritical solutions for particular values of the source Froude number, given by $F_{0b}(\Lambda)$. This curve is also plotted in figure 3. In figures 4, 5 and 6 we illustrate the types of solutions possible when $\Lambda = 0.4$, 1.0 and 2.0.

3.3. *Solutions with drag* ($C_D > 0$) *and finite Froude number at the front*

We now analyse drag-affected gravity currents in the regime for which inertia, buoyancy and drag forces remain of the same magnitude, with a different condition at the front of the current. Rather than specifying the front as the location at which

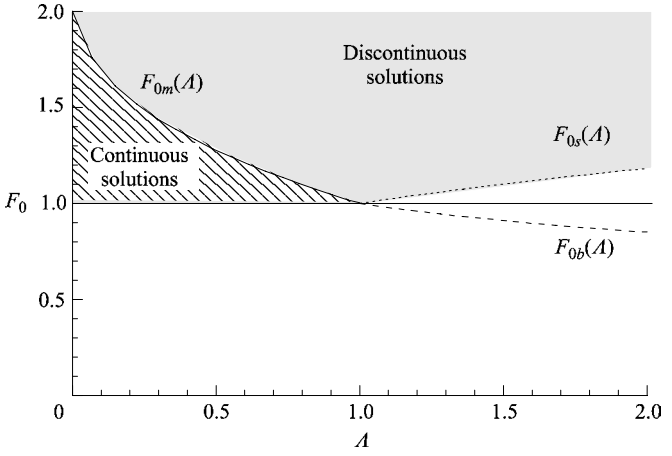

FIGURE 3. The regimes of continuous and discontinuous similarity solutions for inertial gravity currents as functions of the source Froude number F_0 and the drag coefficient Λ. Continuous solutions are possible for $1 \leqslant F_0 \leqslant F_{0m}(\Lambda)$, while discontinuous, supercritical solutions are possible when $F_0 > F_{0m}(\Lambda)$ and $\Lambda < 1$, and when $F_0 > F_{0s}(\Lambda)$ and $\Lambda > 1$. Continuous subcritical solutions exist for $F_0 = F_{0b}(\Lambda)$.

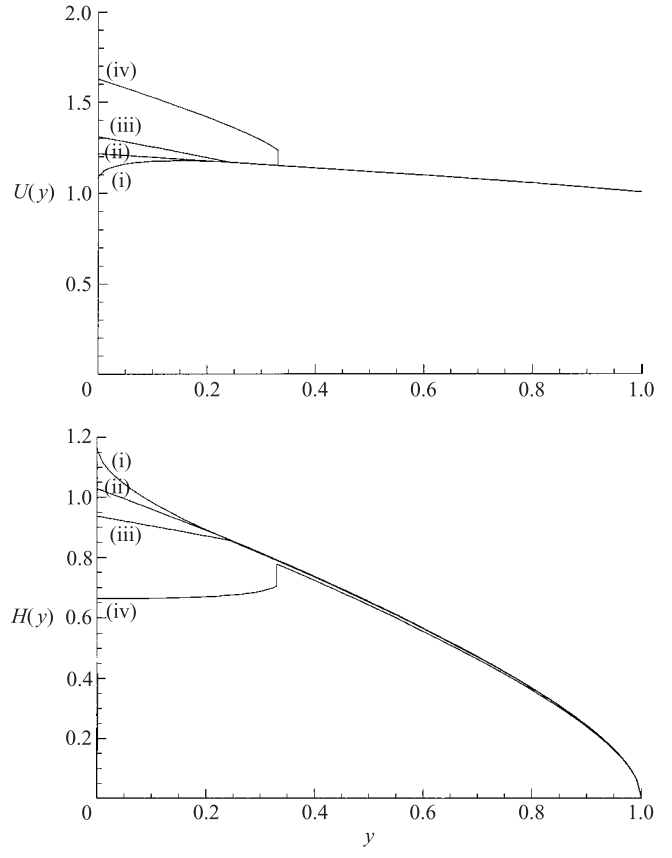

FIGURE 4. The similarity solutions for the height $H(y)$ and velocity $U(y)$ of an inertial gravity current for $\Lambda = 0.4$ as functions of the similarity variable y with various source Froude numbers: (i) $F_0 = 1$, $\lambda = 0.462$; (ii) $F_0 = 1.190$, $\lambda = 0.464$; (iii) $F_0 = 1.353$, $\lambda = 0.467$ and (iv) $F_0 = 2.000$, $\lambda = 0.487$.

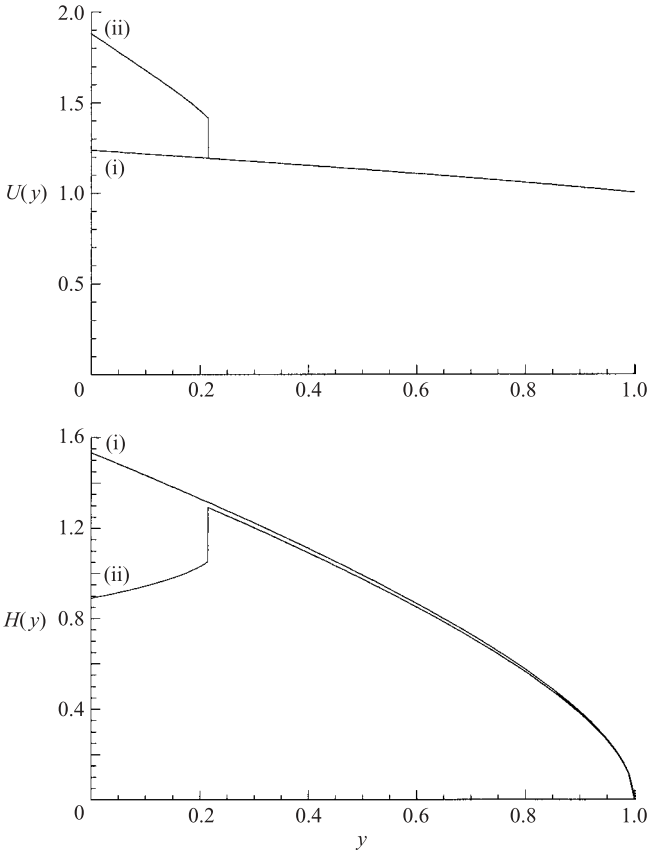

FIGURE 5. The similarity solutions for the height $H(y)$ and velocity $U(y)$ of an inertial gravity current for $\Lambda = 1$ as functions of the similarity variable y with two source Froude numbers: (i) $F_0 = 1$, $\lambda = 0.404$; and (ii) $F_0 = 1.992$, $\lambda = 0.421$.

the height vanishes, we now impose a frontal Froude number given by

$$u = Fr\sqrt{gh} \qquad \text{at} \qquad x = x_f(t). \tag{3.30}$$

The use of this condition is common in the study of Boussinesq gravity currents (Benjamin 1968; Huppert & Simpson 1980; Rottman & Simpson 1983) and in sufficiently deep ambient fluid it is assumed that the Froude number Fr is constant. For example, Huppert & Simpson (1980) suggest that $Fr = 1.2$. (Recall that to apply this analysis to Boussinesq gravity currents we must substitute reduced gravity g' for gravity g.) It is still possible to construct similarity solutions of the form (3.5)–(3.7), but the boundary condition at the front is now given by

$$U = Fr\sqrt{H} \qquad \text{and} \qquad U = 1 \qquad \text{at} \qquad y = 1. \tag{3.31}$$

Gratton & Vigo (1994) systematically explored the types of solution possible in the absence of drag. They showed that for $Fr < 2$ only discontinuous, supercritical solutions may be formed, but for $Fr \geqslant 2$, continuous solutions with points of critical transition are possible provided the Froude number at the source, F_0, satisfies $1 \leqslant F_0 \leqslant 2$.

We calculate solutions when $Fr = 1.2$ for a range of values of the Froude number at the source, F_0, and the drag coefficient, Λ. We plot in figure 7 the regimes in

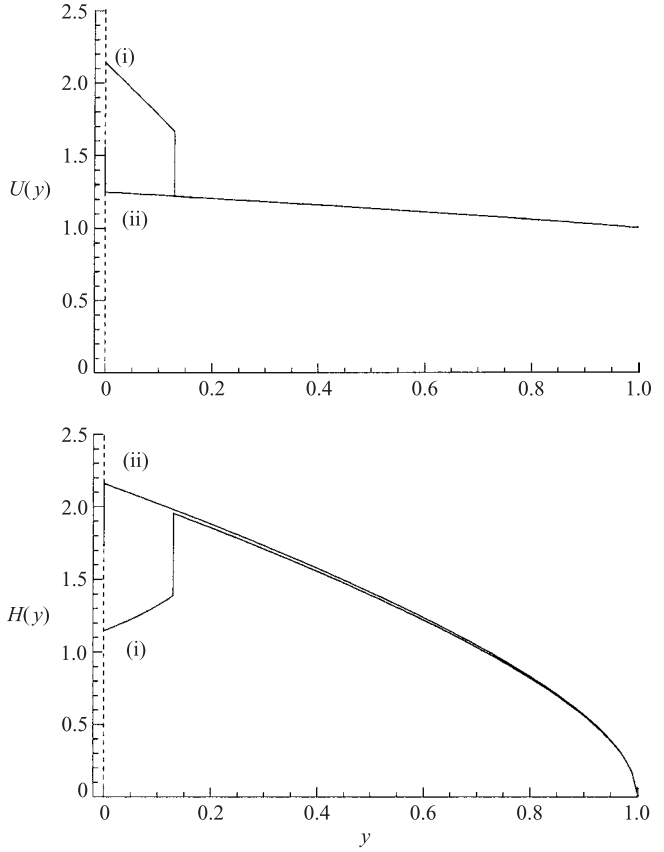

FIGURE 6. The similarity solutions for the height $H(y)$ and velocity $U(y)$ of an inertial gravity current for $\Lambda = 2.0$ as functions of the similarity variable y with two source Froude numbers: (i) $F_0 = 1.184$, $\lambda = 0.359$; and (ii) $F_0 = 2.000$, $\lambda = 0.371$. The solution with $F_0 = 1.184$ has a shock at $y = 0$.

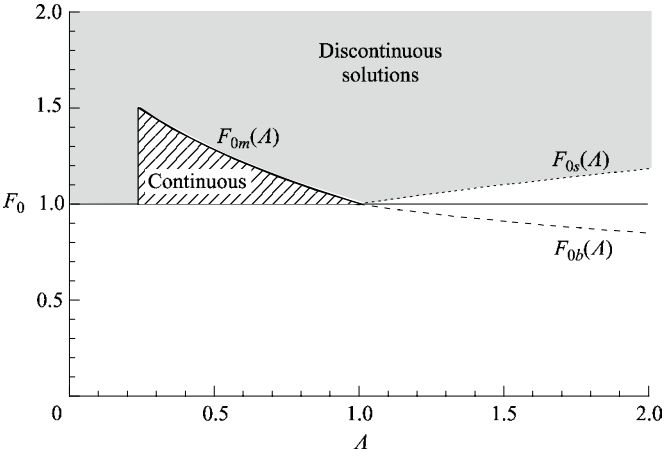

FIGURE 7. The regimes of continuous and discontinuous similarity solutions for inertial gravity currents as functions of the source Froude number F_0 and the drag coefficient Λ when $Fr = 1.2$. Continuous solutions are possible for $1 \leqslant F_0 \leqslant F_{0m}(\Lambda)$, while discontinuous, supercritical solutions are possible when $F_0 > F_{0m}(\Lambda)$ and $\Lambda < 1$, and when $F_0 > F_{0s}(\Lambda)$ and $\Lambda > 1$. Continuous subcritical solutions exist for $F_0 = F_{0b}(\Lambda)$.

which different types of solutions may be constructed. When $\Lambda = 0$, in accord with Gratton & Vigo (1994), we find that only discontinuous solutions are possible. This is most readily established by integrating the governing differential equations, (3.9) and (3.10), from $y = 1$ to a point at which $H = (U - y)^2$, but at which (3.23) is not satisfied. Thus it is not possible to construct continuous solutions. However when $0.241 \leqslant \Lambda \leqslant 1$, we find that it is now possible to construct continuous solutions with points of critical transition, because we can now find a point y_c at which (3.22) and (3.23) are simultaneously satisfied. The boundary between the regimes of continuous and discontinuous solutions is given by a curve $F_{0s}(\Lambda)$, which is identical to the portion of the curve shown in figure 3 for $\Lambda \geqslant 0.241$. Furthermore as in § 3.2, we may only construct discontinuous supercritical solutions when $\Lambda > 1$ and there is the same lower bound on the permissible values of source Froude number, denoted $F_{0m}(\Lambda)$. This corresponds to flows with a shock at the source. There is also the same branch of continuous subcritical solutions, denoted by $F_{0b}(\Lambda)$. The effect of drag, therefore, is to cause the currents to develop steeper gradients close to the fronts of the flows to overcome the drag forces in that region. This then lowers the internal Froude number of the supercritical motion and means that for a sufficiently large drag coefficient it is now possible to find flows that attain critical conditions at some point within their interior so that continuous solutions may be constructed.

3.4. *Modified gravity currents* ($\beta > 1$)

To complete this analysis of the dynamics of gravity currents for which inertia, buoyancy and drag are all of the same order of magnitude, we consider flows in which there is shear in the velocity profile so that the shape factor β exceeds unity. In this case the dimensionless governing equations are the expression for mass conservation (2.2) and the horizontal momentum equation, which is given by

$$\frac{\partial u}{\partial t} + u\frac{\partial u}{\partial x} + g\frac{\partial h}{\partial x} = -C_D\frac{u^2}{h} - 2(\beta - 1)u\frac{\partial u}{\partial x} - (\beta - 1)\frac{u^2}{h}\frac{\partial h}{\partial x}. \tag{3.32}$$

We seek similarity solutions to these equations of the form given by (3.5)–(3.7). In terms of the similarity variables the momentum equation may be written

$$[(U - y + 2(\beta - 1)U]U' + \left[1 + \frac{(\beta - 1)U^2}{H}\right]H' = -\frac{\Lambda U^2}{4\lambda H} - \frac{U}{2}. \tag{3.33}$$

In this subsection, rather than construct solutions to these governing equations and boundary conditions (3.11) and (3.12) for all values of the parameters β, F_0 and Λ, we examine two important facets of the solution. First we seek a series solution in the region close to the front. We find that in the regime $|y - 1| \ll 1$, the similarity solutions are given to leading order by

$$H = \frac{\Lambda}{4\lambda(\beta - 1)}(1 - y) + \ldots \qquad \text{and} \qquad U = 1. \tag{3.34}$$

Note that if $\beta = 1$ then this expression is singular and instead the behaviour close to the front is given by (3.21). In addition if the current is drag-free ($\Lambda = 0$) but $\beta > 1$ then this series solution does not provide the leading-order terms; in fact we find that it is not possible to construct any solution which satisfies the boundary conditions at the front. This phenomenon will be discussed fully in § 5 for dam-break flows; it arises because the characteristic velocity of the governing equations exceeds the fluid speed and so it is not possible to construct solutions with purely kinematic conditions at the front.

We further observe that critical transitions at $y = y_c$ occur when

$$\beta(U_c - y_c)^2 = H_c, \tag{3.35}$$

where $H_c = H(y_c)$ and $U_c = U(y_c)$. This corresponds to a Froude number of $\beta^{-1/2}$, which is less than unity. This departure was discussed by Garrett & Gerdes (2003) and indicates that hydraulically choked conditions occur at Froude numbers less than unity for flows with velocity profiles that include shear. We may also deduce the maximum drag coefficient, Λ_m, for which continuous supercritical flows may be found. This may be shown to be given by

$$\Lambda_m = (2\beta - 1)\beta^{2/3}. \tag{3.36}$$

We note that $\Lambda_m > 1$ when β exceeds unity, reflecting that for flows with velocity shear a larger drag is required to attain critical conditions at the source. Again, this occurs because of the increased characteristic velocity when $\beta > 1$, which will be discussed further in § 5.

4. Dam-break flow

The dam-break solutions to the shallow-water equations emerge as exact solutions to the governing equations (2.2) and (2.3) for $\beta = 1$. The flow corresponds to the one-dimensional motion over a rigid horizontal boundary that results from the sudden release of stationary fluid from behind a vertical barrier (Ritter 1892; Whitham 1974). The initial depth of fluid behind the dam, which is located at $x = 0$, is denoted h_0 and the horizontal surface in front of the dam is initially free of fluid. The solution in the absence of drag is solved by the method of characteristics to give the following height and velocity fields

$$u = \frac{2}{3}\left(\frac{x}{t} + \sqrt{gh_0}\right), \tag{4.1}$$

$$h = \frac{1}{9g}\left(2\sqrt{gh_0} - \frac{x}{t}\right)^2. \tag{4.2}$$

These are valid for $-1 \leqslant x/[t\sqrt{gh_0}] \leqslant 2$ and the position of the front of the flow is given by

$$x_f(t) = 2t\sqrt{gh_0}. \tag{4.3}$$

An alternative view of the dam-break solution is to treat only the flow in $x \geqslant 0$, generated by a constant volume flux per unit width at the origin, $q = 8(gh_0^3)^{1/2}/27$, with the Froude number at the source equal to unity (Gratton & Vigo 1994; Hogg & Woods 2001).

In this solution, basal drag has been neglected on the assumption that $C_D u^2/h \ll g\partial h/\partial x$. While this is valid in the bulk of the flow, close to the front, $x = x_f(t)$, the effects of drag are no longer negligible. Thus there is a region close to the front within which the dynamical balance is different from the rest of the flow. We estimate the extent of this region by balancing the drag and the streamwise pressure gradient. Denoting $\xi = x_f(t) - x$, we find that when $\xi \ll x_f$, $u \sim (gh_0)^{1/2}$ and $h \sim (1/g)(\xi/t)^2$. Thus we deduce that drag is not negligible when

$$\xi^3 \sim C_D g^2 h_0 t^4. \tag{4.4}$$

This scaling for the spatial extent of the drag-affected region yields an identical result to that proposed by Whitham (1955).

In what follows we construct a matched asymptotic expansion for the velocity and height fields. We match between two regions: the 'inner' region, which is located close to the front and within which the drag is non-negligible; and the outer region, which is far from the front and where the dynamics are controlled by a balance between fluid inertia and the streamwise pressure gradient.

We first non-dimensionalize the problem using $(h_0/g)^{1/2}$ and h_0 as time- and lengthscales, respectively. Henceforth all variables will be assumed to be dimensionless. Furthermore we define $\epsilon = C_D^{1/3}$; the expansions are based on the regime $\epsilon \ll 1$.

The outer problem is given by $h = h_d(x,t) + O(\epsilon)$ and $u = u_d(x,t) + O(\epsilon)$, where

$$h_d = \frac{1}{9}\left(2 - \frac{x}{t}\right)^2 \qquad \text{and} \qquad u_d = \frac{2}{3}\left(1 + \frac{x}{t}\right). \tag{4.5}$$

These correspond to the dimensionless dam-break solutions (cf. (4.1) and (4.2)). For the inner region we introduce a scaled spatial coordinate $X = (x_f - x)/\epsilon$, so that the extent of the inner region corresponds to $X = O(1)$, as indicated in the scaling given above. The governing equations are therefore given by

$$\frac{\partial h}{\partial t} + \frac{\dot{x}_f}{\epsilon}\frac{\partial h}{\partial X} - \frac{1}{\epsilon}\frac{\partial}{\partial X}(uh) = 0, \tag{4.6}$$

$$\frac{\partial u}{\partial t} + \frac{\dot{x}_f}{\epsilon}\frac{\partial u}{\partial X} - \frac{u}{\epsilon}\frac{\partial u}{\partial X} - \frac{1}{\epsilon}\frac{\partial h}{\partial X} = -\frac{\epsilon^3 u^2}{h}, \tag{4.7}$$

and the boundary conditions at the front are given by

$$h = 0, \qquad u = \dot{x}_f \qquad \text{at} \qquad X = 0, \tag{4.8}$$

where a dot denotes differentiation with respect to time. Matching to the outer regime demands that $h \to h_d$ and $u \to u_d$ as $X \to \infty$ and so we introduce the following series expansions for the height and velocity fields within the inner region:

$$h = \epsilon^2 H_0(X,t) + \ldots, \tag{4.9}$$

$$u = U_0(X,t) + \epsilon U_1(X,t) + \ldots, \tag{4.10}$$

$$x_f = x_{f0}(t) + \epsilon x_{f1}(t) + \ldots. \tag{4.11}$$

We substitute these series into the governing equations (4.6), (4.7) and equate at each order of ϵ. At $O(1/\epsilon)$, we deduce

$$U_0(X,t) = \dot{x}_{f0}. \tag{4.12}$$

Thus the velocity is independent of X to leading order throughout the inner region close to the front of the flow. (This result was assumed by Whitham (1955) using an integral model, as discussed below.) At $O(1)$ we find that

$$\frac{\partial H_0}{\partial t} + \dot{x}_{f1}\frac{\partial H_0}{\partial X} - \frac{\partial}{\partial X}(U_1 H_0) = 0, \tag{4.13}$$

$$\frac{\partial U_0}{\partial t} = 0. \tag{4.14}$$

The second of these, (4.14), implies that the velocity of the front is constant in time to leading order. Finally at $O(\epsilon)$ from (4.7), we find

$$\frac{\partial U_1}{\partial t} + \dot{x}_{f1}\frac{\partial U_1}{\partial X} - U_1\frac{\partial U_1}{\partial X} - \frac{\partial H_0}{\partial X} = -\frac{U_0^2}{H_0}. \tag{4.15}$$

Matching inner and outer velocity fields yields

$$\frac{2}{3}\left(1+\frac{x_{f0}(t)}{t}\right)=\dot{x}_{f0}. \tag{4.16}$$

Thus the leading-order position of the front is given by $x_{f0}(t)=2t$, as expected from the drag-free dam-break solution. The inner solutions, $H_0(X,t)$ and $U_1(X,t)$, are determined by the solutions to (4.13) and (4.15), subject to the boundary conditions (4.8) and matching to the outer region.

Balancing terms in the momentum equation (4.15) indicates that $H_0/X\sim 1/H_0\sim U_1/t$. Hence we introduce a similarity variable, $\eta=X/[\eta_1 t^{4/3}]$ and seek similarity solutions to (4.15) and (4.13) of the form

$$H_1=\tfrac{16}{9}\eta_1^2 t^{2/3}H(\eta), \tag{4.17}$$

$$U_1=\tfrac{4}{3}\eta_1 t^{1/3}U(\eta), \tag{4.18}$$

$$X_{f1}=\eta_1 t^{4/3}, \tag{4.19}$$

where η_1 is a constant to be determined as part of the solution. (We will show that $\eta_1<0$.) The governing equations (4.15) and (4.13) then become

$$\tfrac{1}{2}H-\eta H'+H'-(UH)'=0, \tag{4.20}$$

$$\tfrac{1}{4}U-\eta U'+U'-UU'-H'=-\frac{81}{64\eta_1^3 H}, \tag{4.21}$$

where a prime denotes differentiation with respect to η. The boundary conditions at $\eta=0$ are given by

$$U(0)=1 \qquad \text{and} \qquad H(0)=0, \tag{4.22}$$

while matching to the outer solution requires that

$$H\to\tfrac{1}{16}(\eta-1)^2 \qquad \text{and} \quad U\to\tfrac{1}{2}(1-\eta) \qquad \text{as} \qquad \eta\to-\infty. \tag{4.23}$$

We numerically integrate these equations, subject to the initial and matching conditions, to determine $U(\eta)$, $H(\eta)$ and η_1. We note that this system of equations includes the possibility of a critical transition where the gradient is discontinuous (cf. § 3). This occurs at positions where $H=(U+\eta-1)^2$ and $U/2+\eta-1=81/[32\eta_1^3 H]$. We plot the height and velocity fields, $H(\eta)$ and $U(\eta)$, in figure 8 and calculate $\eta_1=-2.9976$. The critical point at which the gradients are discontinuous occurs at $\eta=-0.2988$.

We also plot in figure 9 the composite matched asymptotic solution for the drag-affected dam-break solution. In this figure we plot the height and velocity fields, $u(x,t)$ and $h(x,t)$ as functions of x/t. We note that the effects of drag are to retard the flow significantly and to introduce a slightly blunted front to the height profile.

The value of η_1 for the first-order correction to the speed of the dam-break flow is somewhat larger than the value calculated by Whitham (1955), who found that $\eta_1=-2.589$. Whitham (1955) used an integral method, rather than the method of matched asymptotic expansions and hence did not explicitly calculate velocity and height fields within the drag-affected region close to the front of the flow. Using the expansions developed here, however, it is possible to clarify the difference between the two analyses. First we define a position, $\xi_f(t)$, at the outer edge of the inner tip region at the front of the flow, such that $|x_f(t)-\xi_f(t)|\gg\epsilon$. Then mass conservation

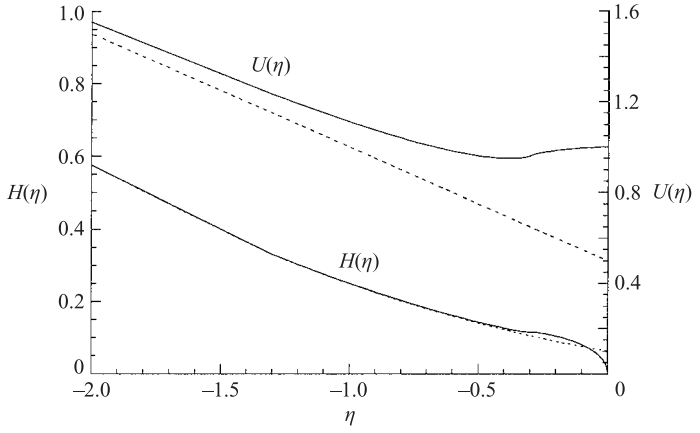

FIGURE 8. The similarity solutions for the height $H(\eta)$ and velocity $U(\eta)$ within the 'inner' region at the front of the dam-break flow, plotted as functions of the similarity variable η (——). Also plotted are the 'outer' height and velocity fields to which these 'inner' fields are matched (- - - -).

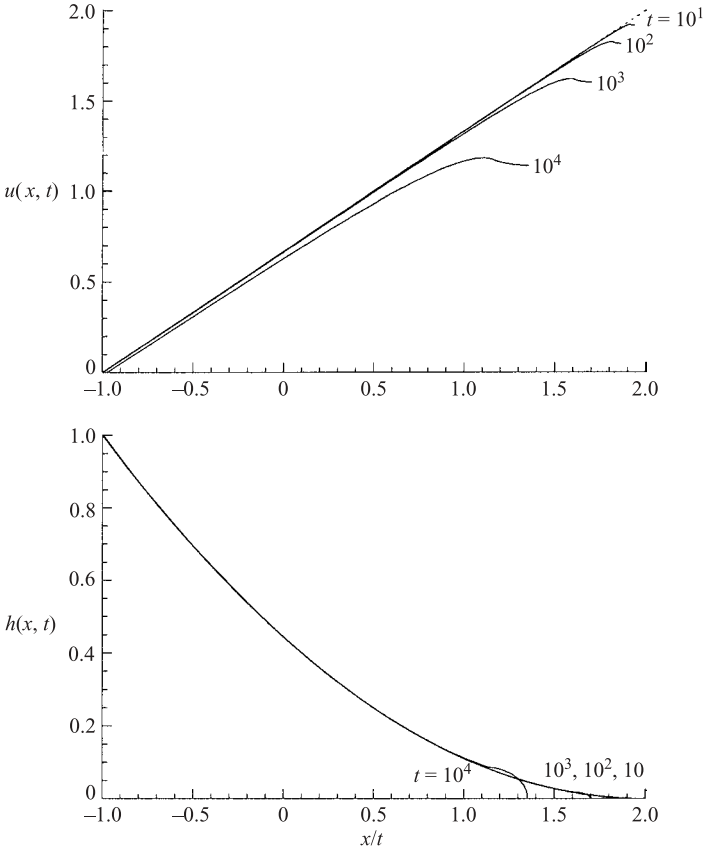

FIGURE 9. The composite solution for the dimensionless height $h(x,t)$ and velocity $u(x,t)$ fields plotted as functions of x/t at $t = 10, 10^2, 10^3$ and 10^4 with $\epsilon = 10^{-2}$ (——). Also plotted is the solution in the absence of drag (- - - -). Note that in the bulk of the domain the height profiles may not be distinguished from the outer solution.

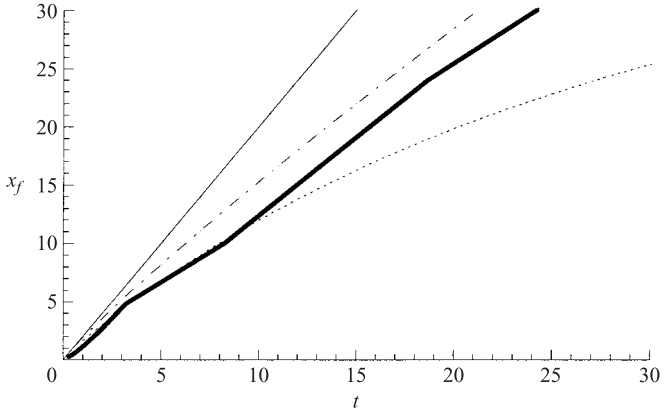

FIGURE 10. Comparisons between the experimentally measured position of the front of the flow as a function of time and the theoretical predictions of Ritter (1892) (——), §4 (- - - -) and §5 (–·–·). The experimental data (▬▬) are from Dressler (1954); they correspond to a dam-break flow of water, arising from an initial dam height of 22 cm and flowing over a smooth-bottomed flume of width 22.5 cm. For the theory of §5, we calculate the parameter values $\beta = 1.017$ and $Y_0 = 0.912$ and the drag coefficient, $C_D = 0.0019$, which are determined from the Reynolds number, $\mathscr{R}$.

yields

$$\frac{\mathrm{d}}{\mathrm{d}t}\int_{\xi_f}^{x_f} h\,\mathrm{d}x = h(\xi_f)\left(u(\xi_f) - \frac{\mathrm{d}\xi_f}{\mathrm{d}t}\right), \tag{4.24}$$

while the integrated momentum equation is given by

$$\frac{\mathrm{d}}{\mathrm{d}t}\int_{\xi_f}^{x_f} hu\,\mathrm{d}x = h(\xi_f)u(\xi_f)\left(u(\xi_f) - \frac{\mathrm{d}\xi_f}{\mathrm{d}t}\right) + \tfrac{1}{2}h^2(\xi_f) - \int_{\xi_f}^{x_f} \epsilon^3 u^2\,\mathrm{d}x. \tag{4.25}$$

Matching the edge of the boundary to the dam-break solutions (4.1) and (4.2) permits the height and velocity, $h(\xi_f)$ and $u(\xi_f)$ to be evaluated, and Whitham (1955) completes the analysis by assuming that the velocity field within the tip region is only a function of time, thus permitting the simple evaluation of the integrals in (4.25). We have found that this is correct to leading order, but at $O(\epsilon)$ there is both spatial and temporal variation (see figure 8). Thus the speed of the front is somewhat overestimated using the approach of Whitham (1955).

The leading-order asymptotic theory may be compared to measurements of dam-break flows in the laboratory. Dressler (1954) conducted a series of relatively large-scale experiments. We estimate the drag coefficient C_D using the empirical formula proposed by Hager (1988) and given by

$$C_D = 0.025\mathscr{R}^{-0.2}, \tag{4.26}$$

where $\mathscr{R} = \rho(gh_0^3)^{1/2}/\mu$. We find that the asymptotic expansion compares well with the laboratory data at early times and is a considerable improvement on the drag-free Ritter solution (see figure 10). We also compare the height profile at a relatively early time and note that the agreement between the theory and experiments is reasonable (figure 11). In the following section, however, we develop a different asymptotic theory and find somewhat improved agreement between the two.

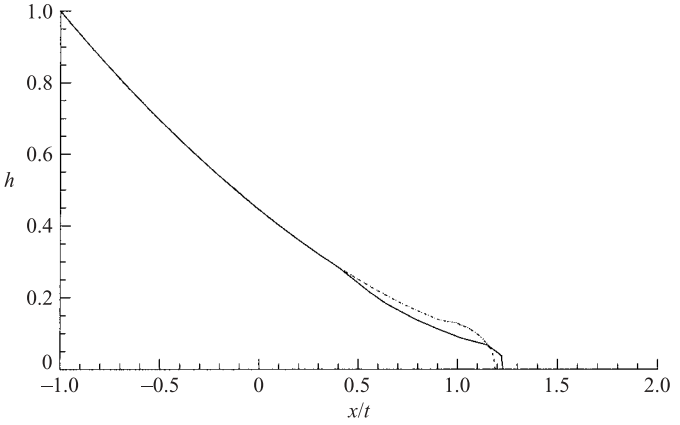

FIGURE 11. Comparisons between the experimentally measured profile of the dam-break flow (——) and the composite expansion (- - - -) as functions of x/t at $t = 13.3$. The experimental data are from Dressler (1954); they correspond to a dam-break flow of water, arising from an initial dam height of 11 cm and flowing over a smooth-bottomed flume of width 22.5 cm.

5. Modified dam-break flow ($\beta > 1$)

We now consider flows for which there is shear in the vertical profiles of the velocity so that the shape factor $\beta > 1$. In the subsection that follows we construct the inviscid solutions to the shallow-water equations and thereafter show how these are modified by resistive forces. Most importantly we find that the structure of the flow is very different when $\beta > 1$ and the dynamical balance within the drag-affected region close to the front of the flow is different from that established in § 4.

5.1. *Dam-break flows in the absence of drag*

We first consider the flow generated in the absence of basal drag by the instantaneous removal of a vertical dam at $x = 0$, behind which fluid is at rest. This solution will form the basis for the matched asymptotic solutions that follow in which drag is only non-negligible within a region close to the front of the flow.

Neglecting drag the dimensionless momentum equation is given by

$$\frac{\partial}{\partial t}(uh) + \frac{\partial}{\partial x}(\beta u^2 h) + \frac{\partial}{\partial x}\left(\frac{h^2}{2}\right) = 0, \tag{5.1}$$

while mass conservation is still given by (2.2). (Here as in § 4, we have non-dimensionalized lengths and times with respect to h_0 and $(h_0/g)^{1/2}$, respectively.) We assume that the shape factor, β, is a function of the velocity and height, $\beta \equiv \beta(u, h)$. For example, it may depend on the local Reynolds number, $\rho uh/\mu$ (see Reynolds & Tiederman 1967). In characteristic form these hyperbolic governing equations are given by

$$\frac{\mathrm{d}h}{\mathrm{d}t} + \gamma_{\pm}\frac{\mathrm{d}u}{\mathrm{d}t} = 0 \qquad \text{on} \qquad \frac{\mathrm{d}x}{\mathrm{d}t} = c_{\pm}, \tag{5.2}$$

where

$$c_{\pm} = \beta u + \tfrac{1}{2}u^2\frac{\partial \beta}{\partial u} \pm \left[u^2\beta(\beta-1) + h + u^3\frac{\partial \beta}{\partial u}\left(\beta - 1 + \tfrac{1}{4}u\frac{\partial \beta}{\partial u}\right) + u^2 h\frac{\partial \beta}{\partial h}\right]^{1/2} \tag{5.3}$$

and

$$\gamma_{\pm} = \frac{h(c_{\pm} - u)}{u^2(\beta - 1) + h + u^2 h\, \partial\beta/\partial h}. \tag{5.4}$$

Thus at the front, as $h \to 0$, the characteristic velocity is equal to the flow speed if $c_+ = u$, which implies that

$$-(\beta - 1)u^2 = u^2 h \frac{\partial \beta}{\partial h}. \tag{5.5}$$

Thus since β remains bounded as $h \to 0$, we deduce that these two velocities are equal only if $\beta(u, h) \to 1$, as $h \to 0$. If the limiting value of β exceeds unity then the characteristic velocity exceeds the front speed and it is not possible to enforce a purely kinematic condition at the front of the flow, as will be discussed below.

Dam-break flow is generated from the initial conditions that at $t = 0$, $h = 1$ for $x < 0$ and $h = 0$ for $x > 0$. The solution is therefore given in terms of simple waves in which the height and velocity fields are functions of x/t (see Whitham 1974). Using the characteristic structure given above, we may calculate the solution for any functional dependence of the shape factor upon the velocity and height fields. For clarity, here we present results for a constant value of β.

The characteristic equation (5.2) on a forward-propagating characteristic may be rewritten as

$$\frac{\mathrm{d}h}{\mathrm{d}u} = -\frac{h((\beta - 1)u + \sqrt{u^2\beta(\beta - 1) + h})}{u^2(\beta - 1) + h}, \tag{5.6}$$

and we may integrate this equation, applying the boundary condition that $h = 1$ when $u = 0$ on each characteristic, to obtain the implicit solution for $\beta > 1$ and $\beta \neq 9/8$:

$$1 = \left[\sqrt{h + \beta(\beta - 1)u^2} + \frac{(3 - 2\beta)}{2}u\right]^{2\beta - 3} h^{3(\beta - 1)} \left[\frac{\sqrt{h + \beta(\beta - 1)u^2} + u\sqrt{\beta(\beta - 1)}}{\sqrt{h + \beta(\beta - 1)u^2} - u\sqrt{\beta(\beta - 1)}}\right]^{\sqrt{\beta(\beta - 1)}}. \tag{5.7}$$

If $\beta = 9/8$ then the solution takes a slightly different form and is given by

$$1 = \frac{1}{8}\exp\left(\frac{2u}{\sqrt{64h + 9u^2} + 3u}\right)(\sqrt{64h + 9u^2} + 3u)^{5/6}(\sqrt{64h + 9u^2} - 3u)^{1/6}. \tag{5.8}$$

Meanwhile, there is a simple-wave expansion fan originating at $x = 0$, $t = 0$ such that

$$\frac{x}{t} = \beta u - \sqrt{h + \beta(\beta - 1)u^2}. \tag{5.9}$$

This solution has some similarity to the classical dam-break solution ($\beta = 1$) and some illustrative solutions are plotted in figure 12. We note from (5.9) that when $u = 0$ and $h = 1$, $x/t = -1$, so the speed with which the expansion fan propagates back into the fluid at rest is independent of β. This is to be expected because inertia is negligible at the point at which the fluid has just started to accelerate.

We also note from (5.7) that if $\beta > 1$, $h \to 0$ only as $u \to \infty$, and it is no longer possible to identify the location of the moving front of the flow. This phenomenon is another manifestation of the fact that the characteristic velocity exceeds the fluid velocity as $h \to 0$. It means that when $\beta > 1$ we can only calculate the position of the front of the flow by explicitly including the effects of drag. This is in contrast to the classical dam-break flow with $\beta = 1$ discussed in the previous section, for which the leading-order position of the front was given by the drag-free solution, $u = 2$ when $h = 0$, and the effect of drag was to introduce a first-order correction to the propagation. However

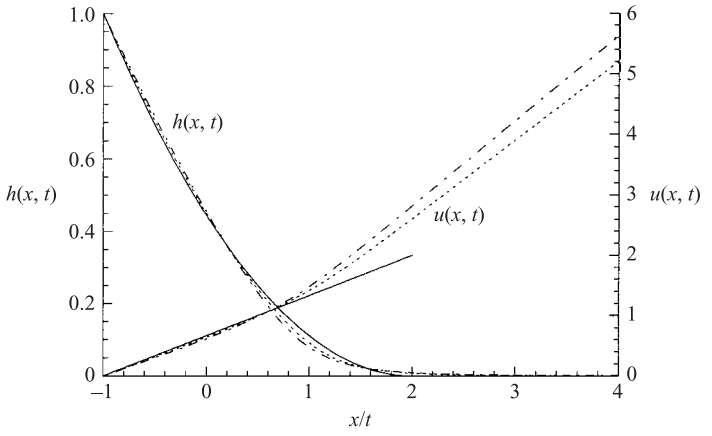

FIGURE 12. The modified dam-break solutions for the height and velocity fields plotted as functions of x/t for $\beta = 1$ (——); $\beta = 1.1$ (- - - -); and $\beta = 1.2$ (– · – · –).

it is physically consistent, since $\beta > 1$ implies that there is shear in the vertical profile of the velocity field, which implies that the flow is necessarily affected by drag forces. Although the solution given by (5.7) and (5.9) was developed for constant β, it is possible to construct a dam-break solution for any $\beta(u, h)$, and the conclusion would be the same for these flows: at the front the characteristic velocity exceeds the flow speed and so it is not possible to identify the location of the front if drag forces are neglected.

From (5.7), we find that as $u \to \infty$,

$$h \sim K_1 u^{-\gamma}, \qquad \text{where} \qquad \gamma = 1 + \sqrt{\frac{\beta}{\beta - 1}}, \tag{5.10}$$

and for $\beta \neq 9/8$

$$K_1^{9-8\beta} = [4\beta(\beta-1)]^{(\beta+3\sqrt{\beta(\beta-1)})}\left[\sqrt{\beta(\beta-1)} + \tfrac{3}{2} - \beta\right]^{(2\beta-3)(3+\sqrt{\beta/(\beta-1)})}, \tag{5.11}$$

while for $\beta = 9/8$

$$K_1 = 256\exp(-2)/81. \tag{5.12}$$

Finally, in the regime $x/t \gg 1$, we obtain the asymptotic behaviour

$$h \sim K_2\left(\frac{x}{t}\right)^{-\gamma} \qquad \text{and} \qquad u \sim \frac{\gamma}{\gamma - 1}\frac{x}{t}, \tag{5.13}$$

where $K_2 = K_1[1 - 1/\gamma]^{\gamma}$. This asymptotic form of the solution will be employed in the matching procedure of the following sections.

5.2. *Dam-break flows with inertial drag*

We now consider how drag forces affect the modified dam-break flow presented above and, in particular, we show that the inclusion of drag permits the front of the flow to be calculated. In this subsection we continue to consider a Chézy model of the drag force, given by (2.5), and so the dimensionless horizontal momentum equation is given by

$$\frac{\partial}{\partial t}(uh) + \frac{\partial}{\partial x}\left(\beta u^2 h + \tfrac{1}{2}h^2\right) = -C_D u^2. \tag{5.14}$$

Since the magnitude of the drag coefficient is small ($C_D \ll 1$), the dam-break solution of § 5.1 provides the leading-order asymptotic solution for the flow away from the front.

However, close to the front, where the depth of the flowing layer becomes small, the effects of drag are non-negligible. In §4 we showed that the leading-order dynamics within the region of the flow close to the front became a balance between the streamwise pressure gradient and the basal drag, because the velocity of the fluid motion was constant to leading order. In the situation now under consideration, this dynamical balance is no longer possible; instead, the leading-order dynamical balance is between the fluid inertia and the drag. This occurs because the inertia of the flow is greater when $\beta > 1$ and so it is not possible to maintain a constant velocity within the tip region.

We may establish the extent of the tip region of the flow by balancing the fluid inertia term $\beta\partial(u^2h)/\partial x$ with the drag $C_D u^2$, while matching to the modified dam-break solution requires that $u \sim x/t$ and $h \sim (x/t)^{-\gamma}$. Thus we deduce that $u = O(C_D^{-1/(\gamma+1)})$ and introduce a rescaled spatial coordinate within the tip region given by $X = (x_f(t) - x)C_D^{1/(\gamma+1)}$. We further pose the following series expansions for the inner height and velocity fields within the inner region:

$$u = C_D^{-1/(\gamma+1)} U_0(X, t) + \ldots, \tag{5.15}$$

$$h = C_D^{\gamma/(\gamma+1)} H_0(X, t) + \ldots, \tag{5.16}$$

$$x_f = C_D^{-1/(\gamma+1)} X_{f0}(t) + \ldots. \tag{5.17}$$

The leading-order terms in the governing equations are then given by

$$\frac{\partial H_0}{\partial t} + \dot{X}_{f0}\frac{\partial H_0}{\partial X} - \frac{\partial}{\partial X}(U_0 H_0) = 0, \tag{5.18}$$

$$\frac{\partial}{\partial t}(U_0 H_0) + \dot{X}_{f0}\frac{\partial}{\partial X}(U_0 H_0) - \beta\frac{\partial}{\partial X}\left(U_0^2 H_0\right) = -U_0^2. \tag{5.19}$$

These equations are subject to the following boundary conditions at the front:

$$U_0(0, t) = \frac{\mathrm{d}X_{f0}}{\mathrm{d}t} \qquad \text{and} \qquad H_0(0, t) = 0. \tag{5.20}$$

Furthermore matching to the outer field yields

$$U_0 \to \frac{\gamma}{\gamma - 1}\frac{X_{f0} - X}{t} \qquad \text{and} \qquad H_0 \to K_2\frac{(X_{f0} - X)^{-\gamma}}{t^{-\gamma}} \qquad \text{as} \qquad X \to \infty. \tag{5.21}$$

This system of equations admits similarity solutions of the form

$$X_{f0} = \frac{\gamma + 1}{\gamma} Y_0 t^{\gamma/(\gamma+1)}, \tag{5.22}$$

$$H_0 = \left(\frac{\gamma + 1}{\gamma} Y_0\right)^{-\gamma} t^{\gamma/(\gamma+1)} H(Y), \tag{5.23}$$

$$U_0 = \frac{\gamma + 1}{\gamma} Y_0 t^{-1/(\gamma+1)} U(Y), \tag{5.24}$$

where the similarity variable is given by $Y = \gamma X/[(\gamma + 1)Y_0 t^{\gamma/(\gamma+1)}]$. Therefore the governing equations are given by

$$H + (1 - Y)H' - \frac{\gamma + 1}{\gamma}(UH)' = 0, \tag{5.25}$$

$$\frac{\gamma - 1}{\gamma} UH + (1 - Y)(UH)' - \frac{\beta(\gamma + 1)}{\gamma}(U^2 H)' = -\frac{\gamma + 1}{\gamma}\left[\frac{(\gamma + 1)Y_0}{\gamma}\right]^{1+\gamma} U^2, \tag{5.26}$$

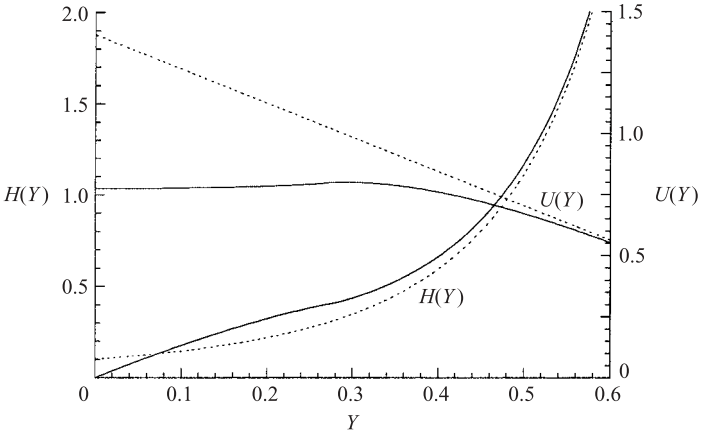

FIGURE 13. The similarity solutions for the height $H(Y)$ and velocity $U(Y)$ within the 'inner' region at the front of the modified dam-break flow subject to inertial drag with $\beta = 6/5$, plotted as functions of the similarity variable Y (——). Also plotted are the 'outer' height and velocity fields to which these 'inner' fields are matched (- - - -).

where a prime denotes differentiation with respect to Y. The boundary conditions are $U(0) = \gamma/(\gamma+1)$ and $H(0) = 0$, while matching to the far field is now given by

$$H \to K_2(1-Y)^{-\gamma} \qquad \text{and} \qquad U \to \frac{\gamma}{\gamma-1}(1-Y) \qquad \text{as} \qquad Y \to 1. \tag{5.27}$$

These equations (5.25)–(5.26) are integrated numerically, with the constant Y_0 being determined as part of the numerical solution. We find that there is an internal critical point at which the gradients of U and H are discontinuous, but the functions themselves are continuous. We plot the functions $U(Y)$ and $H(Y)$ in figure 13, calculated for the case $\beta = 6/5$. In this case the transition occurs at $Y = 0.2694$ and $Y_0 = 0.6242$.

We now compare this leading-order asymptotic theory with laboratory observations of dam-break flow over horizontal, initially dry surfaces; we re-examine the data of Dressler (1954) discussed in the preceding section and we investigate the more recent experiments of Lauber (1997). To apply our new asymptotic theory, we first estimate values of the drag coefficient, C_D, using the empirical expression suggested by Hager (1988). Furthermore we calculate the shape factor β as a function of the Reynolds number $\mathscr{R}$, using the empirical representation of the velocity profile given by Reynolds & Tiederman (1967). For each of the experimental series we calculate β and solve the differential equations to find Y_0. The procedure requires no empirical calibration of the parameters beyond that carried out, using different data, by Reynolds & Tiederman (1967) and Hager (1988).

Comparisons between the theoretical predictions and the experimental measurements are given in figures 10 and 14. We find the agreement between the two is good, and a significant improvement on the drag-free dam-break solution.

It should be noted, however, that this theory is a leading-order expression for the front speed and that we should expect higher-order terms, such as the hydrostatic pressure gradient, to become significant at later times. Furthermore, the theory is hydrostatic; vertical accelerations are assumed to be negligible. This assumption will not hold during the very early phases of the flow. Lauber & Hager (1998) suggest that non-hydrostatic effects are of dynamical significance during the first $\sqrt{2}$ dimensionless

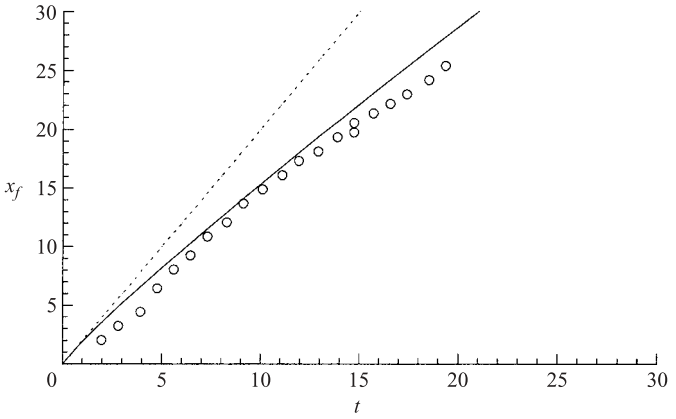

FIGURE 14. The position of the front of the dambreak flow as a function of time. Experimental data (○) are from Lauber (1997) and correspond to an initial dam height of 30 cm within a smooth-bottomed flume of width 50 cm. The theoretical prediction (——) is with $C_D = 0.0018$, $\beta = 1.015$ and $Y_0 = 0.934$. Also plotted is the drag-free solution of Ritter (1892) (– – –).

time units. Indeed, the results presented in figure 14 suggest that an offset of this order to the time-origin of the solutions would improve the agreement between theory and experiment still further; in the absence of a more complete theory of the early phases of the flow, however, we do not employ such a correction.

5.3. *Dam-break flows of Newtonian and power-law fluids with drag*

In this subsection we extend the analysis of these modified dam-break flows to model the 'viscous' drag force due to either a Newtonian fluid or a fluid with a power-law rheology. A depth-averaged horizontal momentum equation for these flows was derived in § 2 and in this context the dimensionless equation is given by

$$\frac{\partial}{\partial t}(uh) + \frac{\partial}{\partial x}\left(\beta u^2 h + \tfrac{1}{2}h^2\right) = -c_n \epsilon_n \left(\frac{u}{h}\right)^n, \tag{5.28}$$

where $\epsilon_n = \tilde{\mu}_n g^{-1+n/2}/[h_0^{1+n/2}\rho]$ and the coefficients β and c_n are functions of the power-law index n (see (2.9)). Recall that a Newtonian fluid corresponds to $n = 1$, while shear-thinning fluids have $n < 1$ and shear-thickening fluids have $n > 1$.

Basal drag is negligible throughout most of these flows since it is assumed that $\epsilon_n \ll 1$. However, as in the preceding subsection, the effects of drag cannot be neglected close to the front where the depth of the flow becomes small, and for the modified dam-break flows it is not possible to identify the front position in the absence of drag. As before, we include the effects of non-negligible drag by forming a matched asymptotic expansion between a region close to the front and the main body of the flow. In the tip region the dynamical balance is between the fluid inertia and the basal drag and we find the following distinguished scalings:

$$u = \epsilon_n^{-1/\alpha} U_0(X, t) + \ldots, \tag{5.29}$$

$$h = \epsilon_n^{\gamma/\alpha} H_0(X, t) + \ldots, \tag{5.30}$$

$$x_f = \epsilon_n^{-1/\alpha} X_{f0}(t) + \ldots, \tag{5.31}$$

where $\alpha = \gamma(n+1)+n-1$ and $X = x_f(t)-x$. In this regime the governing equations to leading order are given by

$$\frac{\partial H_0}{\partial t} + \dot{X}_{f0}\frac{\partial H_0}{\partial X} - \frac{\partial}{\partial X}(U_0 H_0) = 0, \tag{5.32}$$

$$\frac{\partial}{\partial t}(U_0 H_0) + \dot{X}_{f0}\frac{\partial}{\partial X}(U_0 H_0) - \beta\frac{\partial}{\partial X}\left(U_0^2 H_0\right) = -c_n\left(\frac{U_0}{H_0}\right)^n. \tag{5.33}$$

These equations are subject to the same boundary conditions as in the preceding subsection, namely (5.20) and (5.21). We may construct similarity solutions to this system of equations of the form

$$X_{f0} = \frac{\alpha}{\alpha-1} y_0 t^{(\alpha-1)/\alpha}, \tag{5.34}$$

$$U_0 = \frac{\alpha}{\alpha-1} y_0 t^{-1/\alpha} U(y), \tag{5.35}$$

$$H_0 = \left(\frac{\alpha y_0}{\alpha-1}\right)^{-\gamma} t^{\gamma/\alpha} H(y), \tag{5.36}$$

where $\alpha = \gamma(n+1)+n-1$ and the similarity variable $y = X/X_{f0}$. Thence conservation of mass and momentum are given by

$$\frac{\gamma}{\alpha}H + \frac{\alpha-1}{\alpha}(1-y)H' - (UH)' = 0, \tag{5.37}$$

$$\frac{\gamma-1}{\alpha}UH + \frac{\alpha-1}{\alpha}(1-y)(UH)' - \beta(U^2H)' = -c_n\left(\frac{\alpha y_0}{\alpha-1}\right)^{\alpha}\left(\frac{U}{H}\right)^n. \tag{5.38}$$

The matching conditions in terms of these similarity variables are now given by

$$U \to (\gamma/(\gamma-1))(1-y) \qquad \text{and} \qquad H \to K_2(1-y)^{-\gamma} \qquad \text{as} \qquad y \to 1, \tag{5.39}$$

and the boundary conditions are $H(0)=0$ and $U(0)=(\alpha-1)/\alpha$. We integrate these equations numerically using a shooting method to determine y_0. At $y=0$ the right-hand side of (5.38) is singular and so we construct a power-series expansion in the regime $y \ll 1$ and then integrate numerically from $y = y_* \ll 1$. We find that the numerical solution is insensitive to the value of y_* provided it is sufficiently small. In the regime $y \ll 1$ we find that

$$U = \frac{\alpha-1}{\alpha} + \ldots \qquad \text{and} \qquad H = \left[\frac{c_n(n+1)}{\beta-1}\left(\frac{\alpha y_0}{\alpha-1}\right)^{\alpha}\left(\frac{\alpha-1}{\alpha}\right)^{n-2} y\right]^{1/(n+1)} + \ldots. \tag{5.40}$$

This system of equations admits solutions that have critical points at which the height and velocity fields are continuous, but their gradients are discontinuous (cf. § 3).

We have integrated these equations numerically for a range of values of n (see table 1) and we plot the similarity functions for a Newtonian fluid ($n=1$) and for a shear-thinning fluid ($n=1/3$) (figure 15). Although not clearly visible in the height and velocity profiles shown in figure 15, we find that all have a small local maximum in the height fields at the frontal side of the critical point. This corresponds to the small kink in the plotted profiles. The magnitude of this local maximum becomes more pronounced as n decreases.

As before, the most noticeable feature of these profiles is that the current is 'blunt-nosed' with $\partial h/\partial x$ becoming singular at the front of the flow, because fluid piles up

n	β	γ	c_n	$(\alpha-1)/\alpha$	y_c	y_0
1	1.2	3.449	3	0.855	0.259	0.498
3/4	1.176	3.582	2.467	0.834	0.238	0.492
2/3	1.167	3.646	2.305	0.826	0.229	0.491
1/2	1.143	3.828	2	0.809	0.208	0.492
1/3	1.111	4.162	1.710	0.795	0.180	0.507
1/4	1.091	4.464	1.565	0.793	0.163	0.529
1/5	1.077	4.742	1.476	0.796	0.151	0.552
1/10	1.043	5.589	1.282	0.821	0.119	0.656

TABLE 1. Numerically calculated factors for power-law fluids with exponent n; y_c denotes the position at which the critical transition occurs.

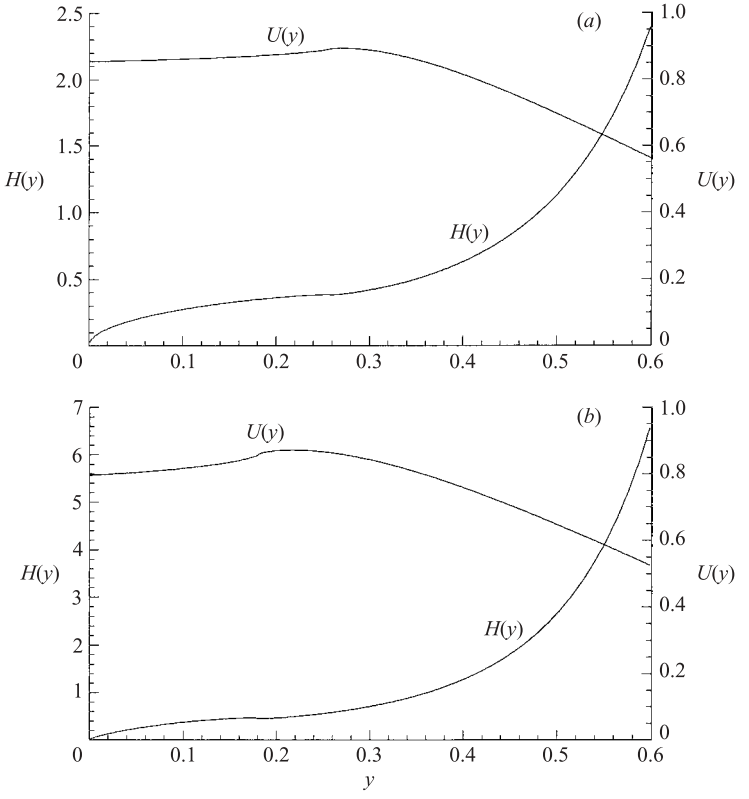

FIGURE 15. The similarity solutions for the height $H(y)$ and velocity $U(y)$ within the 'inner' region at the front of the modified dam-break flow subject to viscous drag plotted as functions of the similarity variable y for (a) Newtonian fluid ($n=1$) and (b) shear-thinning fluid ($n=1/3$).

within the region close to the front where it is decelerated by drag forces. Likewise, the velocity of the flow is reduced and it attains a maximum at some distance behind the front.

As the fluid becomes shear thinning (n decreases from unity), the velocity profile becomes more vertically uniform and the shape factor β decreases towards unity. Consequently, the difference between the frontal and characteristic velocities is reduced. In addition, the drag force becomes more weakly dependent on the height and less

strongly singular as the height diminishes towards the front. Thus the tendency of fluid to accumulate behind the front is also diminished and the profiles are less blunt-nosed. (The height field $h \sim (x_f - x)^{1/(n+1)}$ when $|x_f - x| \ll 1$.)

The rate of propagation of the front is proportional to $t^{(\alpha-1)/\alpha}$, where the exponent $(\alpha-1)/\alpha$ decreases as n is at first reduced from unity, before attaining a local minimum at $n = (2\sqrt{2}-1)/7$ at which the exponent takes the value $(\alpha-1)/\alpha = (3-\sqrt{2})/2$. Thereafter as n decreases further, the exponent increases towards unity. This behaviour is a consequence of the two characteristics of shear-thinning fluid described above. The drag is proportional to $(u/h)^n \sim (x/t)^{(1+\gamma)n}$, which increases as n is reduced from unity because the flow is decelerating. This increased drag means that we expect the rate of propagation to decrease as n decreases from unity. At the same time, as n decreases, the velocity profile becomes more uniform vertically (β becomes closer to unity). As a result, the difference between the characteristic and 'outer' dam-break velocities is reduced and so the extent of the region over which drag forces are significant is also reduced. This results in a smaller reduction of flow speed; hence these two process have opposing effects on the flow speed exponent. We find that initially the increased drag is the dominant effect as n is reduced from unity, but progressively the reduction in the mismatch between the flow and characteristic velocities means that the flow speed exponent increases and approaches unity as $n \to 0$.

6. Conclusions

In this study we have considered the effects of hydraulic resistance on a number of shallow inertial flows over a horizontal rigid boundary. In particular, we have calculated the way in which drag slows the propagation of the fluid front.

For gravity currents supplied by a continuous flux of fluid which increases as t^3, we have developed similarity solutions in which fluid inertia, hydrostatic pressure gradients and hydraulic drag all contribute to the dominant dynamical balance in the flow (§ 3). This somewhat idealized scenario allows us to investigate the control which drag exerts on the form of solutions. One of the most noticeable effects of drag is that the shape of the current is altered close to the front where the current is at its thinnest. In this region, the current is most strongly affected by drag and so it steepens to develop an increased streamwise pressure gradient which counters the hydraulic resistance. We find that the shape of the current is proportional to $(x_f - x)^{1/2}$ as the front is approached. When we permit the horizontal velocity to include shear ($\beta > 1$), we find that it is no longer possible to construct similarity solutions in the absence of drag. We find that it is not possible to satisfy the boundary conditions at the front. This arises because the characteristic velocity exceeds the fluid speed: this is discussed further below in the context of dam-break flows. We also find that the critical conditions are attained at Froude numbers less than unity; this is in accord with the results of Garrett & Gerdes (2003).

As for the drag-free gravity currents described by Gratton & Vigo (1994), our solutions for the height and velocity fields may be continuous, discontinuous, or continuous with a critical transition at which the spatial gradients of velocity and depth are discontinuous. This last possibility in particular seems to be a common feature of inertial flows with drag in which there is a need for an inertially controlled flow at the source to adjust at some point to a partly drag-controlled regime near the front of the current. Indeed, we find that such a transition occurs in all the flows analysed in §§ 4,5.

These flows with a velocity-dependent drag are to be contrasted with those resisted by Coulomb drag (Appendix). Coulomb resistance acts uniformly over the length

of the current and so although it also leads to a somewhat increased pressure gradient, which is necessary to overcome the additional resistance, it does not lead to the severe steepening found with velocity-dependent drag. For gravity currents supplied by a flux of fluid which increases as t^3 we have also constructed similarity solutions for the motion in which the fluid inertia, pressure gradient and Coulomb drag are of the same order of magnitude. These solutions exhibit the same range of behaviour: they may be continuous, discontinuous or continuous with a point of critical transition.

We have also considered dam-break flows, for which we have investigated the effects both of hydraulic drag and of vertical shear in the velocity profile. In such flows, in contrast to the gravity currents of § 3, drag may become significant only in a small region close to the front of the current where the depth becomes small. We have demonstrated how matched-asymptotic expansions may be developed to relate these two dynamical regimes, and used this approach to obtain new leading-order estimates for the effect which drag terms have on the speed of the front.

In the case where the vertical variation of velocity is neglected (§ 4), the dynamical balance close to the front is between drag and the streamwise pressure gradient. Our results are directly comparable to those obtained by Whitham (1955) using less advanced asymptotic techniques. We find that the earlier result underpredicts the reduction of front velocity by around 20%, and that this may be attributed to Whitham's neglect of the spatial variation of velocity in the drag-affected region.

When vertical shear is incorporated, the characteristic structure of the shallow-water equations is substantially altered (§ 5). As a consequence, we find that in the absence of drag it is no longer possible to impose a kinematic boundary condition at the front of the current; rather, drag must be included in order to obtain the leading-order prediction of the front position. We have developed simple-wave solutions in the 'outer' (drag-free) regions, and have again used a matched-asymptotics approach to obtain descriptions of the 'inner' region and estimates of the front speed.

These modified dam-break solutions with drag have some interesting properties. Although the propagation speed of the front is rather different from either the inviscid dam-break solution (Ritter 1892) or the drag-affected solutions considered in § 4, the overall anatomy of the currents is very similar. Away from the front, the free surface forms a convex-upwards expansion wave; while within the front, although the dominant dynamical balance is between fluid inertia and hydraulic drag rather than between hydrostatic pressure gradients and drag, the height profiles of the flows are rather similar to those without vertical shear: a blunt 'toe' with a small local maximum of depth behind it and a point of critical transition behind that. This similarity may be one reason why the significance of the vertical velocity profile has not been remarked upon in previous studies of dam-break and related flows.

Although most of our calculations have been carried out employing a Chézy friction law suitable for turbulent flow, a link may also be made to laminar inertial flows (such as large-scale mudflows) in which the shear profile and drag depend directly on the fluid rheology. We have demonstrated the effect of employing Newtonian and power-law rheologies, using the same matched-asymptotics method as before. For a shear-thinning power-law fluid, it is interesting to examine the competing effects on the front speed as the degree of shear-thinning is varied: for a weakly shear-thinning fluid, drag is increased relative to a Newtonian fluid and thus the speed is reduced, but as the fluid becomes more strongly shear-thinning, the more uniform velocity profile allows the injection of more momentum into the front region, and so increases the front speed again.

We have compared our theoretical predictions to experimental measurements of high-Reynolds-number dam-break flows in the laboratory and have shown that there is quite good agreement between the two. Several issues, however, remain to be investigated experimentally, and we suggest that they may be interesting topics for future laboratory studies. In particular, the results of §§4 and 5 suggest the need for experimental measurements of the vertical profile of the horizontal velocity field; for dam-break experiments performed with non-Newtonian fluids; and for observations with a sufficiently high temporal resolution to permit a full investigation of the initial, and potentially non-hydrostatic, motion. The predictions for drag-affected gravity currents (§3) should also be verified experimentally.

In addition to their interest as fundamental flow problems, these results have direct applications to a range of environmental situations. Dam-break flows in particular are an important model for events ranging from break-out floods to sheet flow events in coastal hydrodynamics, and even in circumstances in which the results presented here are not directly applicable, they provide for the first time a set of analytical predictions against which the output of numerical shallow-water schemes may be validated. They may have a similar role to play in the further investigation of phenomena such as mudflows and debris flows, in which they suggest that the correct resolution of the vertical variation of velocity may be more important than has generally been assumed. In this context, it would also be of interest to extend these results to the systems of hyperbolic equations which result when a yield-stress fluid is modelled in a shallow-water framework (Piau 1996; Mei *et al.* 2002).

Another possible extension of this study would be to investigate the effects of drag-affected dam-break flows as agents of sediment transport, complementing the previous studies by Capart & Young (1998), Fraccarollo & Capart (2002) and Pritchard & Hogg (2002). Some preliminary work on this set of problems has already been carried out Hogg & Pritchard (2003).

Finally, we note that the methods developed in this study could be extended to investigate the effects of drag on some closely related shallow-water flows. A particularly important class of flows represent fluid motion on a sloping beach, either in the context of swash motions driven by breaking waves (Shen & Meyer 1963; Peregrine & Williams 2001) or of the run-up of solitary waves such as tsunamis (Carrier, Wu & Yeh 2003). Insight into the effects of friction in retarding these flows would therefore be of value in a range of physically important situations.

A. J. H. and D. P. acknowledge the financial support of EPSRC. D. P. also acknowledges the financial support of the Newton Trust through the BP Institute, University of Cambridge. Insightful comments from an anonymous referee are gratefully acknowledged.

Appendix. Coulomb drag

In this Appendix we consider the drag-affected motion of shallow flows when the basal drag is modelled as a Coulomb resistance. This approach has been employed in studies of debris flows (Iverson 1997; Iverson & Denlinger 2001) and granular avalanches (Savage & Hutter 1989). In dimensional form the basal drag is given by

$$\tau_b = \frac{\rho g h u \tan\delta}{|u|}, \tag{A 1}$$

where δ is the empirically determined friction angle. For an incompressible flow, conservation of mass is still given by (2.2), while the dimensional streamwise

momentum equation is given by

$$\frac{\partial}{\partial t}(uh) + \frac{\partial}{\partial x}\left(\beta u^2 h + \tfrac{1}{2}gh^2\right) = -\frac{ghu\tan\delta}{|u|}. \tag{A 2}$$

We study two flows with this drag force: the motion of a gravity current for which drag, inertia and buoyancy are of the same order; and dam-break flow.

A.1. *Gravity currents*

By balancing the inertial, pressure gradient and drag terms, we find that it is possible to seek a similarity solution for the motion of the form (3.5)–(3.7). Mass conservation is then given by (2.2), while the streamwise momentum equation with $\beta = 1$ in terms of the similarity variables is given by

$$\tfrac{1}{2}U - yU' + UU' + H' = -\tilde{\epsilon}, \tag{A 3}$$

where $\tilde{\epsilon} = \tan\delta/(4\lambda)$. The boundary conditions are given by (3.11) and (3.12).

The types of solution are similar to those constructed in § 3, namely continuous, continuous with a point of critical transition and discontinuous solutions. First we note that a simple solution is given by

$$U = 1 \qquad \text{and} \qquad H = \left(\tfrac{1}{2} + \tilde{\epsilon}\right)(1 - y). \tag{A 4}$$

At the source ($y = 0$), this solution gives $F_0 = (\tilde{\epsilon} + 1/2)^{-1/2}$ and $\lambda^{-3} = 4(1 + 2\tilde{\epsilon})$. It is also the series solution expansion in the regime $|y - 1| \ll 1$, for all values of F_0 and $\tilde{\epsilon}$. Critical conditions are attained when

$$U_c = 2(y_c + \tilde{\epsilon}) \qquad \text{and} \qquad (H_c - y_c)^2 = H_c, \tag{A 5}$$

where $U_c = U(y_c)$ and $H_c = H(y_c)$. Thus using (A 4) we deduce that $y_c = \frac{1}{2} - \tilde{\epsilon}$. The minimum value of $\tilde{\epsilon}$ for which continuous supercritical solutions may be found corresponds to $y_c = 0$. Thus $\tilde{\epsilon} = 1/2$ and so $\tan\delta = 1$. For values of $\tan\delta$ greater than unity we may only construct discontinuous supercritical solutions, whereas for values of $\tan\delta$ less than unity we may construct continuous and discontinuous solutions. This is analagous to the difficulties encountered in §§ 3.2 and 3.3, where we found that too large a drag coefficient required a discontinuous transition to match the drag-retarded flow near the nose of the current to the supercritical flow at the source.

To construct the continuous solutions we expand $U(y)$ and $H(y)$ in power series for $|y - y_c| \ll 1$. As in § 3 we find that there are two possible series expansions. They are given by

$$U = 1 - \tfrac{1}{2}(y - y_c) - \frac{5}{16(1 + 2\tilde{\epsilon})}(y - y_c)^2 + \ldots, \tag{A 6}$$

$$H = \left(\tfrac{1}{2} + \tilde{\epsilon}\right)^2 - \left(\tfrac{1}{4} + \tfrac{1}{2}\tilde{\epsilon}\right)(y - y_c) - \tfrac{5}{32}(y - y_c)^2 + \ldots \tag{A 7}$$

and

$$U = 1 + a_1(y - y_c)^{5/2} + \ldots, \tag{A 8}$$

$$H = \left(\tfrac{1}{2} + \tilde{\epsilon}\right)^2 - \left(\tfrac{1}{2} + \tilde{\epsilon}\right)(y - y_c) - a_1\left(\tfrac{1}{2} + \tilde{\epsilon}\right)(y - y_c)^{5/2} + \ldots, \tag{A 9}$$

where a_1 is an undetermined constant. Using the first of these expansions to initiate the numerical integration away from the point of critical transition at $y = y_c$ yields the maximum source Froude number $F_0 = F_{0m}(\tan\delta)$ for which continuous solutions may be constructed. Further continuous solutions may be found for $1 \leqslant F_0 < F_{0m}$ using the second series and varying the constant a_1. When $\tan\delta > 1$ there are no

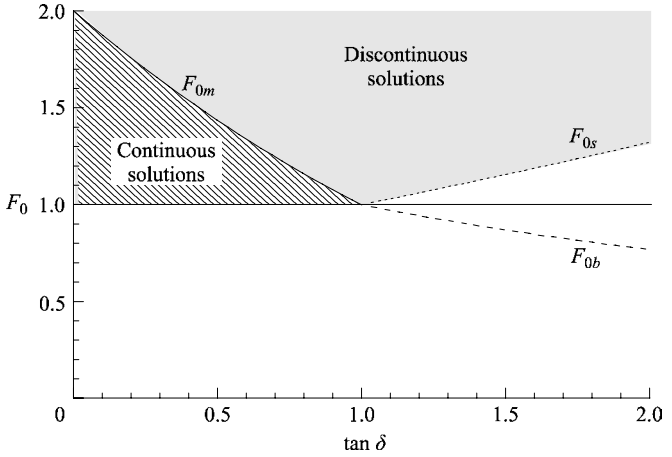

FIGURE 16. Regimes of continuous and discontinuous similarity solutions for inertial gravity currents as functions of the source Froude number F_0 and the Coulomb friction coefficient $\tan\delta$. Continuous solutions are possible for $1 \leqslant F_0 \leqslant F_{0m}(\tan\delta)$, while discontinuous, supercritical solutions are possible when $F_0 > F_{0m}(\tan\delta)$ and $\tan\delta < 1$, and when $F_0 > F_{0s}(\tan\delta)$ and $\tan\delta > 1$. Continuous subcritical solutions exist for $F_0 = F_{0b}(\tan\delta)$.

supercritical continuous solutions, although there is a unique subcritical solution for each value of $\tan\delta$ given by (A 4); this curve is denoted $F_0 = F_{0s}(\tan\delta)$. Furthermore when $\tan\delta > 1$, discontinuous solutions can be found only for $F_0 > F_{0s}(\tan\delta)$, where the flow with source Froude number F_{0s} has a discontinuity at $y = 0$. The regime of possible solutions is shown in figure 16.

A.2. *Dam-break flow*

For dam-break flow, using a lengthscale h_0 and timescale $(h_0/g)^{1/2}$, where h_0 is the initial height of the fluid behind the dam, the dimensionless streamwise momentum equation is given by

$$\frac{\partial}{\partial t}(uh) + \frac{\partial}{\partial x}\left(\beta u^2 h + \tfrac{1}{2}h^2\right) = -\frac{hu\hat{\epsilon}}{|u|}, \tag{A 10}$$

where $\hat{\epsilon} = \tan\delta$.

The form of the drag in (A 10) is very different from the forms investigated in §§4,5. The relative magnitude of the drag does not increase towards the front of the flow and thus its effects are uniform throughout the entire flow. We demonstrate below that when $\beta = 1$ it is simple to calculate how drag retards the front of the flow. However, when $\beta > 1$ we are unable to resolve the problem encountered in §5 of finding the front of the modified dam-break flow. In both cases the effects of drag are spatially uniform so that there is no need to construct matched asymptotic regions within which different force balances govern the motion. We note that both Iverson (1997) and Savage & Hutter (1989) indicate that β should be equal to unity.

When $\beta = 1$, it is simple to write the governing equations (2.2) and (A 2) in characteristic form. This is given by

$$\frac{\mathrm{d}}{\mathrm{d}t}(u + 2\sqrt{h}) = -\frac{\hat{\epsilon}u}{|u|} \qquad \text{on} \qquad \frac{\mathrm{d}x}{\mathrm{d}t} = u + \sqrt{h}, \tag{A 11}$$

$$\frac{\mathrm{d}}{\mathrm{d}t}(u - 2\sqrt{h}) = -\frac{\hat{\epsilon}u}{|u|} \qquad \text{on} \qquad \frac{\mathrm{d}x}{\mathrm{d}t} = u - \sqrt{h}. \tag{A 12}$$

The front, $x_f(t)$, corresponds to the foremost characteristic on which $h=0$. Starting from dam-break initial conditions we find that

$$u = 2 - \hat{\epsilon}t \qquad \text{on} \qquad \frac{\mathrm{d}x_f}{\mathrm{d}t} = u. \tag{A 13}$$

Thus the front is given by

$$x_f = 2t - \tfrac{1}{2}\hat{\epsilon}t^2. \tag{A 14}$$

This is valid provided $u > 0$, which corresponds to $t < 2/\hat{\epsilon}$. At $t = 2/\hat{\epsilon}$ the flow has reached its maximum extent of $x_f = 2/\hat{\epsilon}$.

REFERENCES

Acton, J. M., Huppert, H. E. & Worster, M. G. 2001 Two-dimensional viscous gravity currents flowing over a deep porous medium. *J. Fluid Mech.* **440**, 359–380.

Ancey, C. 2002 Debris flows and related phenomena. In *Geomorphological Fluid Mechanics* (ed. N. J. Balmforth & A. Provenzale). Lecture Notes in Physics. Springer.

Batchelor, G. K. 1967 *An Introduction to Fluid Dynamics*. Cambridge University Press.

Bellos, C. V. & Sakkas, J. G. 1987 One-dimensional dam-break flood-wave propagation on dry bed. *J. Hydraul. Engng* **113**, 1510–1524.

Benjamin, T. B. 1968 Gravity currents and related phenomena. *J. Fluid Mech.* **31**, 209–248.

Capart, H. & Young, D. L. 1998 Formation of a jump by the dambreak wave over a granular bed. *J. Fluid Mech.* **372**, 165–187.

Carrier, G. F., Wu, T. T. & Yeh, H. 2003 Tsunami run-up and draw-down on a plane beach. *J. Fluid Mech.* **475**, 79–99.

Coussot, P. & Proust, S. 1996 Slow, unconfined spreading of a mudflow. *J. Geophys. Res.* **101**, 25217–25229.

Dressler, R. F. 1952 Hydraulic resistance effect upom the dam-break functions. *J. Res. Natl Bur. Stand.* **49**, 217–225.

Dressler, R. F. 1954 Comparison of theories and experiments for the hydraulic dam-break wave. In *Publication 38 de l'Association Internationale d'Hydrologie*, pp. 319–328.

Fraccarollo, L. & Capart, H. 2002 Riemann wave descriptions of erosional dam-break flows. *J. Fluid Mech.* **461**, 183–228.

Garrett, C. & Gerdes, F. 2003 Hydraulic control of homogeneous shear flows. *J. Fluid Mech.* **475**, 163–172.

Gratton, J. & Vigo, C. 1994 Self-similar gravity currents with variable inflow revisited: plane currents. *J. Fluid Mech.* **258**, 77–104.

Hager, W. H. 1988 Abflussformeln für turbulente Strömungen. *Wasserwirtschaft* **78**, 79–84.

Hallworth, M. A., Hogg, A. J. & Huppert, H. E. 1998 Effects of external flow on compositional and particle gravity currents. *J. Fluid Mech.* **359**, 109–142.

Hatcher, L., Hogg, A. J. & Woods, A. W. 2000 The effects of drag on turbulent gravity currents. *J. Fluid Mech.* **416**, 297–314.

Hogg, A. J. & Pritchard, D. 2003 Suspended sediment transport by drag-affected dam-break flow. In *Proc. Rivers, Coastal and Estuarine Morphodynamics 2003* (ed. A. Sánchez-Arcilla & A. Bateman). IAHR.

Hogg, A. J. & Woods, A. W. 2001 The transition from inertia to drag-dominated motion of turbulent gravity currents. *J. Fluid Mech.* **449**, 201–224.

Hoult, D. P. 1972 Oil spreading on the sea. *Annu. Rev. Fluid Mech.* **2**, 341–368.

Huang, X. & Garcia, M. H. 1998 A Herschel-Bulkley model for mud flow down a slope. *J. Fluid Mech.* **364**, 305–333.

Hunt, B. 1987 An inviscid dam-break solution. *J. Hydraul. Res.* **25**, 313–327.

Huppert, H. E. & Simpson, J. E. 1980 The slumping of gravity currents. *J. Fluid Mech.* **99**, 785–799.

Iverson, R. M. 1997 The physics of debris flows. *Rev. Geophys.* **35**, 245–296.

Iverson, R. M. & Denlinger, R. P. 2001 Flow of variably fluidized granular masses across three-dimensional terrain 1. coulomb mixture theory. *J. Geophys. Res.* **106** (B1), 537–552.

Keulegan, G. H. 1950 Wave motion. In *Engineering Hydraulics* (ed. H. Rouse), pp. 711–768. Chapman & Hall.

Lauber, G. 1997 Experimente zut Talsperrenbruchwelle im glatten geneigten Rechteckkanal. Ph. D. thesis, Technischen Hochschule, Zurich.

Lauber, G. & Hager, W. H. 1998 Experiments to dambreak wave: Horizontal channel. *J. Hydraul. Res.* **36**, 291–307.

Lewis, R. 1997 *Dispersion in Estuaries and Coastal Waters*. Wiley.

Mei, C. C., Liu, K. F. & Yuhi, M. 2002 Mud flow – slow and fast. In *Geomorphological Fluid Mechanics* (ed. N. J. Balmforth & A. Provenzale). Lecture Notes in Physics. Springer.

Ng, C. & Mei, C. C. 1994 Roll waves on a shallow layer of mud modelled as a power-law fluid. *J. Fluid Mech.* **263**, 151–183.

Parker, G. 1976 On the cause and characteristic scales of meandering and braiding in rivers. *J. Fluid Mech.* **76**, 457–480.

Parker, G., Fukushima, Y. & Pantin, H. M. 1986 Self-accelerating turbidity currents. *J. Fluid Mech.* **171**, 145–181.

Peregrine, D. H. 1972 Equations for water waves and the approximations behind them. In *Waves on Beaches and Resulting Sediment Transport* (ed. R. Meyer), Chapter 3, pp. 95–121. Academic.

Peregrine, D. H. & Williams, S. M. 2001 Swash overtopping a truncated plane beach. *J. Fluid Mech.* **440**, 391–399.

Piau, J. M. 1996 Flow of a yield stress fluid in a long domain. Aplication to flow on an inclined plane. *J. Rheology* **40**, 711–723.

Pritchard, D. & Hogg, A. J. 2002 On sediment transport under dambreak flow. *J. Fluid Mech.* **449**, 265–274.

Reynolds, W. C. & Tiederman, W. G. 1967 Stability of turbulent channel flow, with application to Malkus's theory. *J. Fluid Mech.* **27**, 253–272.

Ritter, A. 1892 Die Fortpflanzung der Wasserwellen:. *Z. Vereines Deutsch. Ing.* **36** (33), 947–954.

Rottman, J. W. & Simpson, J. E. 1983 Gravity currents produced by instantaneous releases of heavy fluid in a rectangular channel. *J. Fluid Mech.* **135**, 95–100.

Savage, S. B. & Hutter, K. 1989 The motion of a finite mass of granular material down a rough incline. *J. Fluid Mech.* **199**, 177–215.

Shen, M. C. & Meyer, R. E. 1963 Climb of a bore on a beach. Part 3. Run-up. *J. Fluid Mech.* **16**, 113–125.

Simpson, J. E. 1997 *Gravity Currents in the Environment and the Laboratory*. Cambridge University Press.

Stansby, P. K., Chegini, A. & Barnes, T. C. D. 1998 The intial stages of dam-break flow. *J. Fluid Mech.* **374**, 407–424.

Weir, G. J. 1983 The asymptotic behaviour of simple kinematic waves of finite volume. *Proc. R. Soc. Lond.* A **387**, 459–467.

Whitham, G. B. 1955 The effects of hydraulic resistance in the dambreak problem. *Proc. R. Soc. Lond.* A **227**, 399–407.

Whitham, G. B. 1974 *Linear and Nonlinear Waves*. Wiley.